Journal of Structural Dynamics, 5, (pp. 1-30) 2026
Local Models to Identify the Nonlinear Behavior of a Bolted Joint

Journal of Structural Dynamics

Local Models to Identify the Nonlinear Behavior of a Bolted Joint

Cody R Greener *[1], Matthew S Allen †[2], and Raymond Joshua[3]

[1] *Graduate Student, Brigham Young University, Department of Mechanical Engineering*
[2] *Professor, Brigham Young University, Department of Mechanical Engineering*
[3] *Senior Mechanical Engineer, Kansas City National Security Campus*

Abstract

Previous studies have shown that one can create an efficient model for bolted structures by spidering the interface to a pair of nodes, and then connecting them with a nonlinear Iwan element. However, no method has been developed for predicting the parameters of the Iwan element from first principles; in all studies to date, experimental vibration measurements have been acquired and optimization has been used to solve for the Iwan parameters that best reproduce the measurements. This work investigates an alternative strategy that uses a local finite element model in which the bolt and surrounding area are modeled in detail with contact, Coulomb friction and the applied preload. A series of static loads are then applied to this local model and the resulting nonlinear force-displacement behavior is extracted and used to identify either a linear spring or an Iwan element that captures the predicted behavior. The identified springs and Iwan elements are then inserted into a reduced-order model of the structure, and the effective, amplitude-dependent natural frequency and damping of several modes of the structure can be computed, or dynamic transient analysis performed. This work evaluates the proposed modeling strategy using two-dimensional models of cantilever beams containing one and three bolts. In each case, the frequency and damping behavior of the reduced order models, whose Iwan elements were identified using the proposed procedure, are compared those of a truth model. The results show that, while each bolt in a structure can be loaded quite differently, the proposed procedure provides a reasonable approximation to the damping behavior of a joint, predicting the average nonlinear damping in the system within a factor of 1.5-3.

Keywords: nonlinear joints; system identification; Iwan element; frictional joint

Received on April 26, 2026, *Accepted on August 6, 2026*, *Published on August 20, 2026*

1 Introduction

Finite element models (FEM) are a powerful tool for predicting the behavior of a design without the need for physical testing, making them a cost-effective alternative to experimental approaches in the design process. Despite these advantages, simulations also have important limitations, one of the most significant being computational cost. Large models, complex geometries, and nonlinear physics can all drastically increase the computational burden. A common and particularly challenging example is the bolted joint. Accurately capturing bolt behavior requires fine meshes, contact constraints, and frictional interactions, and in large assemblies with many bolts this quickly becomes computationally prohibitive. Beyond their computational cost, bolted joints play a critical role in the energy dissipation of structural systems. As a structure vibrates, contact interfaces within the joint experience micro-slip, which can significantly damp the overall response. Under sufficiently large loads, the joint may also enter macro-slip, where the contact surfaces slide relative to one another. This behavior not only alters the dynamic response of the structure, but can also be detrimental to joint integrity and may ultimately lead to failure.

*grecody@byu.edu
†matt.allen@byu.edu

One approach developed to more efficiently model joints was introduced in 2013 by Festjens et al. [1]. In their approach, a finely meshed local model of the joint is coupled with a coarser mesh of the full structure. The local model retains the detailed joint geometry and nonlinear physics, such as friction, that are removed from the global model. The two models are then iteratively coupled until the total strain energy of the bolt converges. This strategy offered improved computational cost while retaining good accuracy, particularly in capturing nonlinear joint behavior. At the same time, the approach requires a specialized computational framework to manage the iterative exchange between global and local models. (Although global/local modeling or submodeling has been explored in a variety of works [2].) Festjens et al. were also the first to propose a quasi-static approach to characterize the behavior of one mode of the assembled structure at a time, which was far less computationally expensive than a dynamic analysis. In essence, a distributed quasi-static load is applied in the shape of a selected mode to activate only that mode of interest. The amplitude of the applied load is then increased over the range of interest, and either the strain and dissipated energies [1] or the load-displacement curves [3] are used to extract the effective natural frequency and damping behavior of the mode in question.

Lacayo and Allen [3] presented a similar approach, which also used quasi-static analysis to speed up predictions for the nonlinear behavior of a single mode, and which was later found to be a special case of the method of Festjens et al. [1].[1] The primary difference was that Lacayo and Allen treated the entire FEM as nonlinear, so that one did not need to iterate between the linear and nonlinear subdomains. Lacayo and Allen called this method Quasi-Static Modal Analysis (QSMA), and subsequent works found that it could be used to efficiently predict the amplitude-dependent damping of a variety of structures [6, 7], although the cases studied had only a few bolted joints. When a structure has many joints, it would be attractive to be able to model each type of joint separately using a local model, as proposed in [1]. Furthermore, it would be advantageous to use a simplified, reduced-order model for each of the joints, rather than having to simultaneously solve a highly detailed local model.

This problem has been addressed in industrial applications by using spidering or multi-point constraints (MPCs) to connect all of the nodes in the vicinity of a joint to a single linear or nonlinear element that represents the joint [8]; this allows one to greatly reduce the fidelity of the mesh near the joint. Indeed, Lacayo and Allen's first work on QSMA [3] applied it to a model in which spidering had been used to reduce the joints to a pair of nodes with a single Iwan element [9] between them. Hurty/Craig–Bampton (HCB) reduction can then be used to speed up simulations [10, 11, 12]. In Lacayo's work and in some subsequent works [13, 14], model updating was used to determine the parameters of the joints (i.e. the parameters of the Iwan elements that captured motion in the slip direction and the linear spring stiffnesses for those directions that were treated as linear) to bring the model into agreement with experimental measurements. In other words, the method was not predictive but a way of deriving a reduced order model when experimental measurements are available. It would be very useful to have a means of predicting the Iwan parameters of a joint when a structure is modeled in this way, because this approach scales to realistic structures with hundreds of joints [15].

The objective of this work is to investigate an alternative strategy for deriving simplified models for joints, wherein the parameters of the Iwan elements are derived from a quasi-static simulations on a finite element model (FEM) of a single joint in isolation, referred to as a local model. This approach removes the need for direct calibration to experimental measurements, and yet it is designed to be compatible with global dynamics models in which spiders are used to reduce the joints to pairs of nodes. To evaluate the accuracy of the proposed approach, the behavior of the ROM is compared to a high fidelity truth model, where QSMA is used to derive the true behavior for each mode. Specifically, we compare how well each model predicts the amplitude-dependent frequency and damping behavior of bolted assemblies. The proposed approach is far less involved than the local-global modeling approach proposed by Festjens et al. [1], yet it does involve several approximations which simplify the procedure and yet could affect the accuracy of the results. The proposed approach is outlined in Sec. 2. The models that it is applied to are described in Sec. 3, and the results obtained when implementing this with two different local models are reported in Sec. 4.

Furthermore, in order to evaluate the proposed approach, a high fidelity truth model is used to predict the joint force-displacement characteristics of the truth model in Sec. 5. The ROM performance is then examined to provide insight into how local joint behavior relates to the accuracy and predictive capability of the reduced-order model.

[1] Allen and Lacayo's work was first presented in [4]. Baek and Epureanu also independently proposed a related method at about the same time [5].

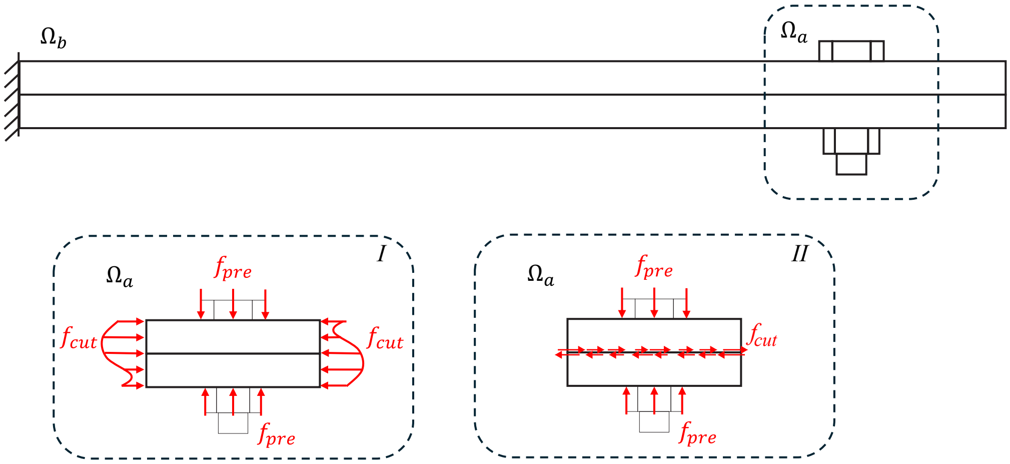

Fig. 1: Representation of a bolted structure being partitioned into a local domain model, Ω_a and a global domain model, Ω_b. In the local domain, preload forces, $\mathbf{f}_{\text{pre}}$, are depicted being applied from the tension in the bolt. In addition, in (I) the internal boundary forces, $\mathbf{f}_{\text{cut}}$, are also represented, corresponding to the forces transmitted from the global model, Ω_b. An alternative set of internal forces is shown in (II).

2 Theory

2.1 Formulating the Local Model

To capture the nonlinear behavior of a joint, this work begins by considering the approach of Festjens et al. [1], who proposed an iterative framework that partitions a finely meshed finite element model of the joint from the remainder of the structure. In this formulation, the joint is represented as the local domain Ω_a, while the surrounding structure is modeled with a coarser mesh to reduce computational cost and is denoted as domain Ω_b. See Figure 1 for a depiction of these domains.

Starting from the general nonlinear equation of motion,

$$\mathbf{M}\ddot{\mathbf{u}} + \mathbf{K}\mathbf{u} + \mathbf{f}_{\text{int}}(\mathbf{u}, \boldsymbol{\theta}) = \mathbf{f}_{\text{ext}}, \tag{1}$$

where $\mathbf{M}$ and $\mathbf{K}$ are the mass and stiffness matrices, $\mathbf{u}$ is the displacement vector, $\mathbf{f}_{\text{ext}}$ represents externally applied forces, and $\mathbf{f}_{\text{int}}$ denotes the nonlinear interface forces, which depend on the displacements and could also depend on the past history of the displacements, which are captured in $\boldsymbol{\theta}$. Other forms of damping are not included at this stage. Partitioning this system into the two domains gives

$$\begin{bmatrix} \mathbf{M}_{aa} & \mathbf{M}_{ab} \\ \mathbf{M}_{ba} & \mathbf{M}_{bb} \end{bmatrix} \begin{Bmatrix} \ddot{\mathbf{u}}_a \\ \ddot{\mathbf{u}}_b \end{Bmatrix} + \begin{bmatrix} \mathbf{K}_{aa} & \mathbf{K}_{ab} \\ \mathbf{K}_{ba} & \mathbf{K}_{bb} \end{bmatrix} \begin{Bmatrix} \mathbf{u}_a \\ \mathbf{u}_b \end{Bmatrix} + \begin{Bmatrix} \mathbf{f}_{\text{int}} \\ \mathbf{0} \end{Bmatrix} = \begin{Bmatrix} \mathbf{f}_{\text{pre}} \\ \mathbf{f}_{\text{ext}} \end{Bmatrix}, \tag{2}$$

where subscripts a and b denote the local and global domains, respectively. Here, $\mathbf{f}_{\text{pre}}$ represents bolt preload forces that act only on Ω_a, and $\mathbf{f}_{\text{ext}}$ corresponds to external loads applied to Ω_b. The interface forces, $\mathbf{f}_{\text{int}}$, come from friction and are contained within the Ω_a domain.

The goal is to find a set of loads and boundary conditions that one can apply to Ω_a so that it can be solved without considering Ω_b. The conditions should be such that the solution, i.e. $\mathbf{u}_a$ and $\ddot{\mathbf{u}}_a$, is identical to that which would be obtained by solving Eq. (2). Festjens et al. [1] proposed an iterative algorithm in which the local model, Ω_a, is solved and then the boundary displacements and forces are passed to the model Ω_b, which is linear. Iteration continues until the forces and displacements in the local model match those in the global model. In each iteration, nodes may stick or slip in the nonlinear local model Ω_a, changing the forces and displacements at the interface and hence influencing the global model. They also recognized that the local model could be considered to behave quasi-statically if the rest of the structure was moving in a single mode of vibration.

The present work does not employ this iterative procedure developed by Festjens et al. but instead seeks to find a set of quasi-static loads and boundary conditions that one can apply to the local model Ω_a to obtain an adequate approximation of the motion $\mathbf{u}_a$ of the region Ω_a in the full model.

Focusing on the top row of Eq. (2), which corresponds to the local domain Ω_a, yields

$$\begin{bmatrix}\mathbf{M}_{aa} & \mathbf{M}_{ab}\end{bmatrix}\begin{Bmatrix}\ddot{\mathbf{u}}_a\\ \ddot{\mathbf{u}}_b\end{Bmatrix} + \begin{bmatrix}\mathbf{K}_{aa} & \mathbf{K}_{ab}\end{bmatrix}\begin{Bmatrix}\mathbf{u}_a\\ \mathbf{u}_b\end{Bmatrix} + \mathbf{f}_{\text{int}} = \mathbf{f}_{\text{pre}}. \tag{3}$$

The coupling terms associated with the Ω_b domain can be condensed into internal forces acting across a cut at the interface. Specifically,

$$-\mathbf{M}_{ab}\ddot{\mathbf{u}}_b - \mathbf{K}_{ab}\mathbf{u}_b = \mathbf{f}_{\text{cut}}, \tag{4}$$

where $\mathbf{f}_{\text{cut}}$ denotes the restoring forces transmitted through the cut. These forces can also be seen depicted in Figure 1. Then substituting this into Eq. (3) allows the joint to be expressed in terms of applied and internal forces, without explicit dependence on the global domain, Ω_b. The governing equation of the local joint then becomes

$$\mathbf{M}_{aa}\ddot{\mathbf{u}}_a + \mathbf{K}_{aa}\mathbf{u}_a + \mathbf{f}_{\text{int}} = \mathbf{f}_{\text{pre}} + \mathbf{f}_{\text{cut}}. \tag{5}$$

This equation shows that, once the surrounding structure is removed, its influence on the local model must be replaced by appropriate external loading. In the approach of Festjens et al. [1], these loads are obtained through an iterative coupling between the local and global models. The present work instead considers an independently constructed local model and seeks a practical loading strategy that identifies the nonlinear force-displacement behavior required by the reduced-order model without performing this iterative procedure.

An independently constructed local model, denoted by $\tilde{\mathbf{K}}_{aa}$, is created by extracting a portion of the geometry from the full model; it is not extracted as a partition of the global model's mass and stiffness matrices, as was done by Festjens et al. [1]. Consequently, the stiffness matrix of the local model does not contain the stiffness contributions from the surrounding structure.[2]

Since the disconnected local model is no longer coupled to the surrounding structure, the interface loading transmitted by Ω_b is no longer directly available. Moreover, the objective of this work is not to reproduce the exact distribution of forces acting across the cut boundary. Multiple loading distributions may produce essentially the same local deformation of the joint.[3] Consequently, this work adopts a practical loading strategy that applies quasi-static loads directly to the local model to identify the nonlinear force-displacement behavior associated with each spring in the reduced-order model. The applied loads are therefore chosen to be consistent with the ROM representation rather than to reproduce the detailed internal forces of the cut boundary. The equivalent loading used for each local analysis is described in Sec. 2.2.

To establish the connection between the local model, nonlinear modal behavior, and the reduced-order model (ROM), and the reduction techniques presented in [13, 16, 14] are reviewed in Sec. 2.2 and QSMA [3] is briefly reviewed in Sec. 2.4.

2.2 Reduced Order Model

The governing Equation (1) can also be used to create a reduced order model. In this work, there is only one master FEM and both the ROM and the local models are extracted from it. However, in practice a ROM would actually be created from a model that has a much lower fidelity mesh near the joints. Also, the ROM would initially not have any nonlinear features, such as contact and friction, so we can consider $\mathbf{f}_{\text{int}}(\mathbf{u}, \boldsymbol{\theta}) = 0$ at this stage. Let us denote the nodes at the surface, where the part interfaces with other parts, as $\mathbf{u}_S$.

[2]For example, consider three nodes [1,2,3] that are connected by springs k_{12} and k_{23}. If domain Ω_a consists of nodes 1 and 2, then $\mathbf{K}_{aa} = [k_{12}, -k_{12}; -k_{12}, (k_{12} + k_{23})]$. In contrast, if we began with a local model that was not connected to Ω_b, the stiffness matrix would be $\tilde{\mathbf{K}}_{aa} = [k_{12}, -k_{12}; -k_{12}, k_{12}]$

[3]Imagine a cantilever where the tip is deflected downward 1 mm. One could achieve that by applying a point load at the tip, a distributed load over the beam, a force and moment at the tip or by loads at several locations simultaneously.

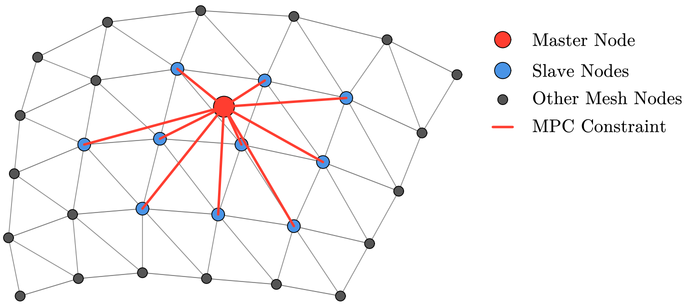

Fig. 2: Visualization of a multi-point constraint or spider.

Multi-point constraint (MPC) spider elements are then applied to each of the contact surfaces, condensing the interfaces into a single master node [3, 13, 16]. Figure 2 shows a schematic of a typical MPC. There are multiple types of MPCs that may be used, but they all have a similar form. An averaging-type constraint (called an RBE3 in Nastran® or a Continuum Distributing constraint in Abaqus®) defines a matrix $\mathbf{R}_{\text{RBE3}}$ that is used to estimate the displacements of the jth master node (given a subscript B) from those of the jth surface (subscript S).

$$\mathbf{u}_B^j = \mathbf{R}_{\text{RBE3}}\mathbf{u}_S^j \tag{6}$$

In a 2D model, each master node $\mathbf{u}_B^j$ has three degrees of freedom (DOF), two translations and one rotational DOF. So $\mathbf{R}_{\text{RBE3}}$ is $3 \times N_S$, where N_S represents the number of slave nodes. The entries of the first row of $\mathbf{R}_{\text{RBE3}}$ would simply be $[\frac{1}{N_S}, 0, \frac{1}{N_S}, 0, ...]$ so that the first row of the product $\mathbf{R}_{\text{RBE3}}\mathbf{u}_S^j$ gives the average displacement of the slave nodes in the first direction. Similarly, $\mathbf{R}_{\text{RBE3}}$ is constructed so that the rotation of the master node matches the average rotation of the slave nodes. For a 3D model, $\mathbf{R}_{\text{RBE3}}$ would be $6 \times N_S$, where each node has three translational and three rotational DOFs.

Any forces applied to the interface node are mapped to those of the surface using a similar relationship. The process to do so is somewhat more involved, but is described in detail in [17] and in the theory manuals for other finite element packages.

Once each of the interfaces has been reduced to a single master node, all of the master DOF can be collected into a vector $\mathbf{u}_B = \left[\left(\mathbf{u}_B^{(1)}\right)^{\mathrm{T}}, \left(\mathbf{u}_B^{(2)}\right)^{\mathrm{T}}, ...\right]^{\mathrm{T}}$. These are the boundary nodes in a Hurty/Craig-Bampton [10, 11, 12] reduction. The governing equations, Eq. (1), are then rearranged to separate the boundary nodes, $\mathbf{u}_B$, and internal nodes, $\mathbf{u}_I$ as follows.

$$\begin{bmatrix} \tilde{\mathbf{M}}_{BB} & \tilde{\mathbf{M}}_{BI} \\ \tilde{\mathbf{M}}_{IB} & \tilde{\mathbf{M}}_{II} \end{bmatrix} \begin{Bmatrix} \ddot{\mathbf{u}}_B \\ \ddot{\mathbf{u}}_I \end{Bmatrix} + \begin{bmatrix} \tilde{\mathbf{K}}_{BB} & \tilde{\mathbf{K}}_{BI} \\ \tilde{\mathbf{K}}_{IB} & \tilde{\mathbf{K}}_{II} \end{bmatrix} \begin{Bmatrix} \mathbf{u}_B \\ \mathbf{u}_I \end{Bmatrix} = \begin{Bmatrix} \mathbf{f}_B \\ \mathbf{f}_I \end{Bmatrix}, \tag{7}$$

where the subscripts B and I denote the boundary and internal DOFs, respectively. The tilde over each matrix emphasizes the fact that we began with a model for the local system that is not connected to Ω_b. The system is reduced using the Hurty/Craig-Bampton [10, 11, 12] transformation,

$$\begin{Bmatrix} \mathbf{u}_B \\ \mathbf{u}_I \end{Bmatrix} = \mathbf{T}^{HCB} \begin{Bmatrix} \mathbf{u}_B \\ \mathbf{q}_m \end{Bmatrix} = \begin{bmatrix} \mathbf{I} & \mathbf{0} \\ \mathbf{\Psi} & \mathbf{\Phi} \end{bmatrix} \begin{Bmatrix} \mathbf{u}_B \\ \mathbf{q}_m \end{Bmatrix}. \tag{8}$$

Briefly, the first column of the transform, $\begin{bmatrix} \mathbf{I} & \mathbf{\Psi}^{\mathrm{T}} \end{bmatrix}^{\mathrm{T}}$, represents the constraint modes, which capture the static response of the structure when each boundary DOF is displaced by a unit amount. The second column, $\begin{bmatrix} \mathbf{0} & \mathbf{\Phi}^{\mathrm{T}} \end{bmatrix}^{\mathrm{T}}$, represents the fixed-interface modes, or the modes of the structure when all boundary nodes are held fixed. This transformation is applied to Eq. (7), the result is,

$$\begin{bmatrix} \hat{\mathbf{M}}_{BB} & \hat{\mathbf{M}}_{BI} \\ \hat{\mathbf{M}}_{IB} & \mathbf{I} \end{bmatrix} \begin{Bmatrix} \ddot{\mathbf{u}}_B \\ \ddot{\mathbf{q}}_m \end{Bmatrix} + \begin{bmatrix} \hat{\mathbf{K}}_{BB} & \mathbf{0} \\ \mathbf{0} & \mathbf{\Omega}_{\text{FB}}^2 \end{bmatrix} \begin{Bmatrix} \mathbf{u}_B \\ \mathbf{q}_m \end{Bmatrix} = \begin{Bmatrix} \mathbf{f}_B \\ \mathbf{0} \end{Bmatrix}, \tag{9}$$

where $\mathbf{q}_m$ and $\mathbf{\Omega}_{\mathbf{FB}}^{\mathbf{2}}$ are, respectively, the modal coordinates and a diagonal matrix of natural frequencies squared, both associated with the fixed-interface modes. $\mathbf{I}$ is the identity matrix. Now, the boundary nodes (each the center of a spider) can be connected using nonlinear elements. Let $\mathbf{f}_{\text{nl}}(\mathbf{u}_B, \boldsymbol{\theta})$ denote the vector of forces defining the nonlinear elements. In this work, Iwan elements [9] are used to connect the interface nodes in certain directions. In particular, the directions that are parallel to the interface surface. That way, the Iwan spring will be used to characterize the nonlinear behavior that is inherent in the sticking and slipping on the interface. The force in each Iwan element depends on the displacement across the joint, and the past history of the displacement of the state of all of the sliders used to model the element [18]. The final equations governing the reduced model then become,

$$\begin{bmatrix} \hat{\mathbf{M}}_{BB} & \hat{\mathbf{M}}_{BI} \\ \hat{\mathbf{M}}_{IB} & \mathbf{I} \end{bmatrix} \begin{Bmatrix} \ddot{\mathbf{u}}_B \\ \ddot{\mathbf{q}}_m \end{Bmatrix} + \begin{bmatrix} \hat{\mathbf{K}}_{BB} & \mathbf{0} \\ \mathbf{0} & \boldsymbol{\Omega}_{\text{FB}}^2 \end{bmatrix} \begin{Bmatrix} \mathbf{u}_B \\ \mathbf{q}_m \end{Bmatrix} + \begin{Bmatrix} \mathbf{f}_{\text{nl}}(\mathbf{u}_B, \boldsymbol{\theta}) \\ \mathbf{0} \end{Bmatrix} = \begin{Bmatrix} \mathbf{f}_B \\ \mathbf{0} \end{Bmatrix}. \tag{10}$$

Linear springs are also inserted between the boundary nodes in the normal and rotational directions, so there would be additional entries in the matrices above for those springs. For a more detailed explanation of HCB reduction, see [12].

Note that, while the surface, $\mathbf{u}_S$ and interfaces $\mathbf{f}_{\text{int}}$ typically comprise a large number of nodes, the HCB boundary nodes $\mathbf{u}_B$ comprise only 3 or 6 DOF per node, so this set is always relatively small.

It is important to note that, while the HCB reduced equations of motion in Eq. (10) have a similar form to the global/local equations of motion in Eq. (2), there are some important differences. The DOF $\mathbf{u}_a$ in the local model consists of all DOF of that model, nodes at the boundary, interface and internal to the local model. In contrast, the boundary DOF of the HCB model $\mathbf{u}_B$ are a relatively small set. Granted, those boundary DOF are related to the motion of a larger set of nodes over the contact interface via Eq. (6). This prompts the question, is there a set of forces $\mathbf{f}_{\text{cut}}$ that could be applied to Eq. (5) to obtain a model for the forces in the nonlinear joint models $\mathbf{f}_{\text{nl}}(\mathbf{u}_B, \boldsymbol{\theta})$, which act between each pair of interface nodes? The approach used in this work is outlined in Sec. 2.3.

2.3 Identifying Nonlinear Joints in the Reduced Order Model (ROM)

This work proposes a procedure for identifying the behavior of a joint for use in the ROM by extracting the force–displacement relationship from the local model governed by Eq. (5). The central challenge is that the true interaction between the joint and the surrounding structure occurs through an unknown distribution of internal stresses acting along the cut boundary, represented by $\mathbf{f}_{\text{cut}}$. These distributed forces are not directly available and depend on the global structural response.

However, in the ROM described by Eq. (10), the global structure interacts with the joint only through a small set of discrete degrees of freedom located at the master nodes of the spider elements. The ROM does not resolve the force distribution at the interface; instead, the joint only responds to the resulting forces and moments transmitted through the generalized degrees of freedom located at the spider master nodes. Hence, this work proposes to use the local model to determine the relationship between these resultant loads and the relative motion across the interface.

To enable direct comparison with the ROM, the same RBE3 spider elements used in the global model are introduced into the local model. For interface surfaces j and k, the corresponding master node displacements are defined as

$$\mathbf{u}_{a_B}^j = \mathbf{R}_{\text{RBE3}}^j \mathbf{u}_{a_S}^j, \qquad \mathbf{u}_{a_B}^k = \mathbf{R}_{\text{RBE3}}^k \mathbf{u}_{a_S}^k, \tag{11}$$

where $\mathbf{u}_{a_S}^j$ and $\mathbf{u}_{a_S}^k$ are the displacement vectors of the nodes on the opposing contact surfaces of the local model.

The relative motion across the joint, which defines the kinematic measure used to characterize the joints force-displacement behavior, is then defined as

$$\mathbf{u}_r = \mathbf{u}_{a_B}^j - \mathbf{u}_{a_B}^k. \tag{12}$$

The RBE3 elements introduce no stiffness, therefore, they do not alter the mechanical response of the local model; they only provide a kinematic reduction consistent with the ROM representation to measure the corresponding motion in the ROM.

As discussed previously, when the local model is extracted from the full structure, the effect of the surrounding structure can be replaced with $\mathbf{f}_{\text{cut}}$ forces at the boundaries, which take the place of the internal stresses that would normally transmit forces from the surrounding structure. On the other hand, if the local model is created with free boundary conditions, i.e. a stiffness matrix $\tilde{\mathbf{K}}_{aa}$ as defined earlier, a different set of forces would be needed to cause the local model to correctly approximate the kinematics of the joint. In either case, the forces on the system would be expected to vary spatially over the boundary of the system, and they cannot be readily defined for a general case. Indeed, the work of Festjens et al. [1] shows that there is tight coupling between these forces, the global model and the relaxation that occurs in the local model as the joint slips. On the other hand, a ROM replaces the force and displacement at the joint with a scalar force and moment that are applied to a single node representing the joint, and then transmitted to the surrounding structure by the MPC spider.

How can these seemingly disparate approaches be related? One can represent the net mechanical effect of the true force distribution on the local model with an equivalent resultant force and moment,

$$\mathbf{F}_{\text{eq}} = \int_{\Gamma} \mathbf{f}_{\text{cut}}(\mathbf{r}_{\text{cut}})\, d\Gamma, \qquad \mathbf{M}_{\text{eq}} = \int_{\Gamma} (\mathbf{r}_{\text{cut}} - \mathbf{r}_B) \times \mathbf{f}_{\text{cut}}(\mathbf{r}_{\text{cut}})\, d\Gamma, \tag{13}$$

where $\mathbf{r}_B$ is the reference location of the spider master node, $\mathbf{r}_{\text{cut}}$ is the location on the cut surface and Γ is the cut surface. These relationships could be used to compute an equivalent force and moment to apply to the master node of the spider, which would approximate a known distributed force $\mathbf{f}_{\text{cut}}$.

In practice, the force $\mathbf{f}_{\text{cut}}$ is not known, so this work uses the reverse approach. An arbitrary force $\mathbf{F}_{\text{eq}}$ is applied to the master node of the spider, and the local model distributes this according to a spider that is defined to match that used in the ROM. For a 2D system, one need only apply force in the tangential direction, so $\mathbf{f}_{\text{cut}}$ is simply a scalar and a range of values can be applied to characterize the behavior of the joint. This approach is shown schematically in Fig. 1 pane II. Alternatively, a scalar force and moment can both be applied, although in this case one must determine the relative strength of each, as is discussed later.

Note that this approximation affects only how the local model is loaded. The local model itself retains the full nonlinear contact and friction behavior at the joint interface, so the internal mechanics of the joint are still resolved in detail. To identify an Iwan model approximating its nonlinear behavior, the local model is subjected to a sequence of quasi-static load steps in which equivalent forces and moments are applied at the spider master nodes. For each load step, the resulting relative displacement $\mathbf{u}_r$ is computed, producing a force–displacement curve for the joint. These curves represent the effective behavior that the ROM experiences when load is transmitted through the joint. The nonlinear springs in the ROM are then parameterized to reproduce this measured relationship. The linear springs are also parameterized by finding the slope of the force-displacement response in the corresponding direction.

In this work, two force loading strategies are considered. The first approach, referred to as the *Pure Shear Local Model*, applies a single resultant load aligned with the degree of freedom associated with the spring being identified. Separate quasi-static analyses are performed for each translational and rotational DOF represented in the ROM. The load is incrementally increased until the joint approaches macro-slip, and the corresponding force–displacement response is recorded. Three examples can be seen in Figure 3 for a 2D case with only three degrees of freedom. The responses in the normal (Figure 3(b)) and rotational (Figure 3(c)) directions are expected to be linear over the range of interest, so the nonlinear modeling focuses on the shear in the joint.

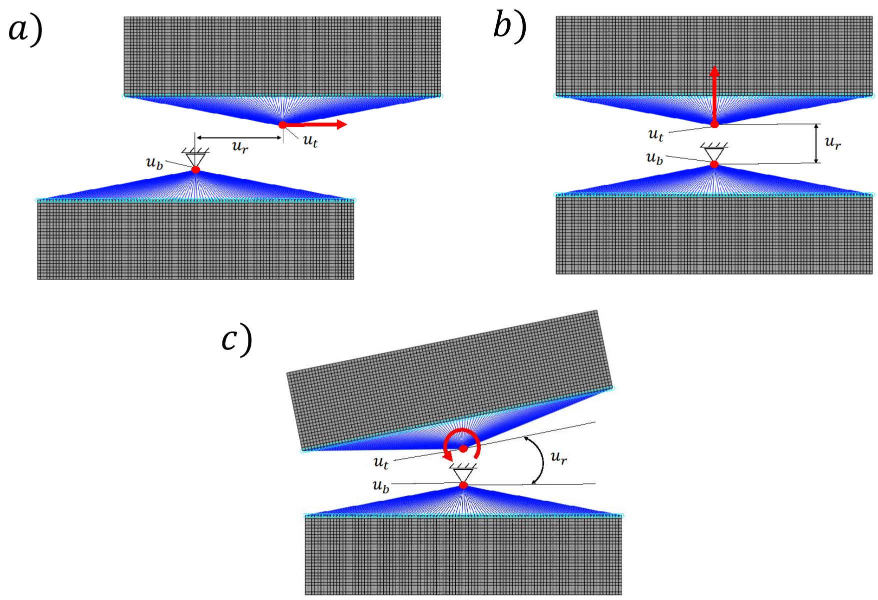

Fig. 3: Finite element mesh of a **local model** shown in an exploded view to illustrate the RBE3 spiders and their reference points. In the actual configuration, the upper and lower members are in contact. The master nodes related to the nodal displacements u_t and u_b are also located on the top and bottom contact-surface nodes without an offset. The relative tangential displacement is defined as $u_r = u_t - u_b$. a) is configured to tune a spring in the horizontal direction with a force that is parallel with the interface. b) is configured for a spring in the vertical direction with a vertical force. c) has an applied moment to tune a rotational spring.

The second approach, referred to as the *Shear-Moment Local Model*, applies a combined force and moment intended to better approximate the coupling effect between the two loads. In this formulation, the equivalent moment is assumed proportional to the applied force,

$$M_{\text{eq}}\alpha = F_{\text{eq}}, \tag{14}$$

where α is a proportionality parameter representing an effective moment arm. This produces a more general loading state that can capture coupling between translation and rotation at the interface. This approach does add additional complexity by requiring a defined relationship between the two loads. Currently, this approach would not be nearly as predictive as the first approach since the ideal proportionality parameter would not be known.

The two loading strategies represent different approximations of the unknown boundary forces, $\mathbf{f}_{\text{cut}}$. Neither reproduces the exact force distribution field that would arise in the full structure, but both provide a practical means of extracting joint behavior that is compatible with the reduced representation used in the ROM. Their relative performance is evaluated in the results presented later.

The procedure proposed in this paper is summarized in Fig. 4. Beginning with the drawings of the structure of interest, one creates two models. The first is a local model in which the bolt area is modeled in detail including the preload force applied to the joint and friction at the contact interface. The second model is a simplified representation of the global model, in which the bolt is replaced with an MPC spider. This model is linear and excludes the preload forces, friction and contact; those effects are captured by inserting linear springs and an Iwan element between the contacting surfaces. The same RBE3 spiders used in the ROM are also added to the local model, a force can be applied at the joint and so the displacement and force can be extracted. The resulting load-displacement cures are used to identify an Iwan element that reproduces the stick-slip behavior of the joint. The parameters of the Iwan element are then inserted in to the ROM of the global structure so one can predict the dynamic response of the structure. One can also use quasi-static modal analysis [3] to predict the amplitude dependent frequency and damping of each mode of the structure, as reviewed in the next section.

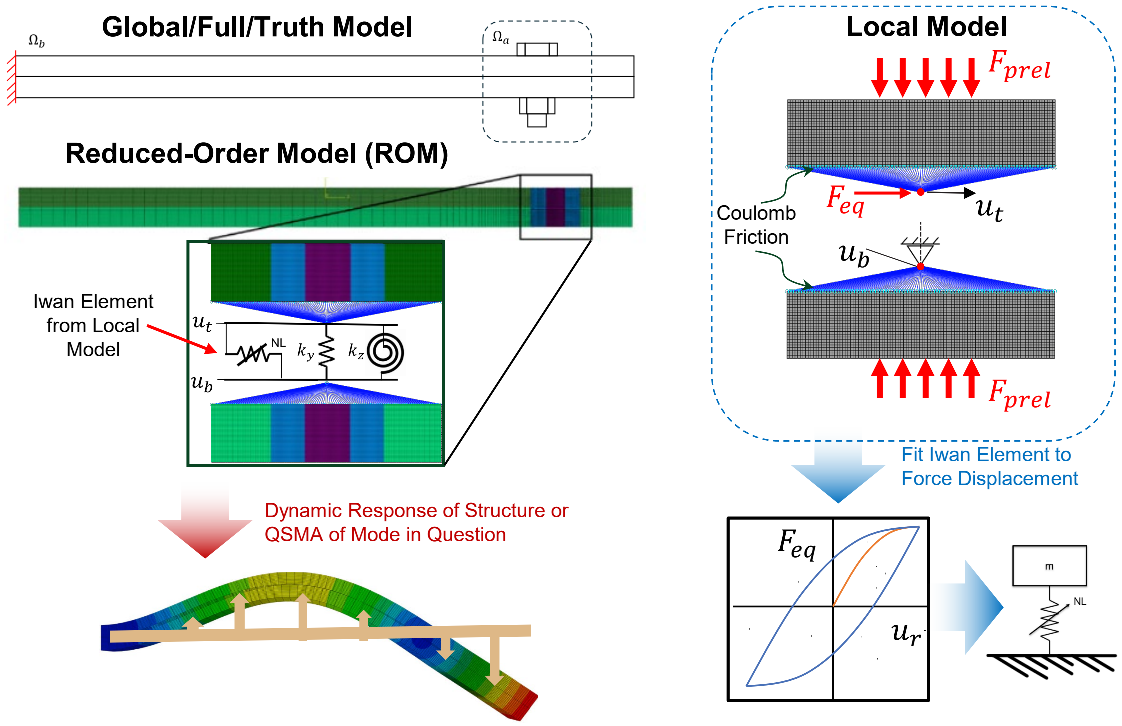

Fig. 4: Overview of the workflow proposed in this paper: 1.) Beginning with a global model of a structure with a joint, 2.) Create a local model of the joint, including the preload force and friction between the surfaces. Add RBE3 spiders to extract the net force and displacement in the surface. 3.) Identify an Iwan element approximating the joint from the force-displacement data. 4.) Create a ROM of the structure with RBE3 spiders to a pair of nodes for the interface. Insert the Iwan element into the model for any similar joints. 5.) Perform dynamic analysis or QSMA on the ROM to predict the structure's response.

Note that the ROM contains a nonlinear Iwan element, so it is a nonlinear model, and hence requires an iterative solution. In this work, a nonlinear quasi-static solver is used, based on Newton's method, to solve for the quasi static response of the ROM and then quasi-static modal analysis is applied to relate this to the dynamic response. One can also use the Newmark-Beta method to integrate the dynamic equations of the ROM; the authors have applied this approach to this type of ROM in other works (see, e.g. [3]).

2.4 Quasi-Static Modal Analysis and Nonlinear Modal Dynamics

Quasi-Static Modal Analysis (QSMA), developed by Lacayo and Allen [3], provides a computationally efficient method to extract the nonlinear modal behavior of a structure without requiring time-consuming transient simulations. QSMA applies a series of quasi-static forces that excite a single mode in isolation. Specifically, a load distribution proportional to a selected mode shape is applied to Eq. (1) as

$$\mathbf{f}_{\text{ext}} = \beta \mathbf{M} \mathbf{\Phi}_r, \tag{15}$$

where $\mathbf{f}_{\text{ext}}$ is the applied load, $\mathbf{\Phi}_r$ is the rth mass normalized mode shape, and β is a scaling factor that gradually amplifies the load. This procedure forces the structure to respond nonlinearly along the chosen modal direction, as illustrated in the bottom of Figure 4. At each load step, the amplitude-dependent stiffness and damping properties are computed using Masings assumptions [1, 3]. This is done by building a force-displacement curve from each of the load steps to define a full hysteresis loop. The secant line stiffness of the curve corresponds to the amplitude-dependent natural frequency, $\omega_r(\beta)$, and the area enclosed by the loop is the energy dissipated per cycle, D, which defines the damping.

$$\omega_r(\beta) = \sqrt{\frac{\beta}{q_r(\beta)}}, \tag{16}$$

and

$$\zeta_r(\beta) = \frac{D(\beta)}{2\pi(q_r(\beta)\omega_r(\beta))^2}, \tag{17}$$

where $\omega_r(\beta)$ and $\zeta_r(\beta)$ are the amplitude-dependent natural frequency and damping and q_r is the modal amplitude.

In prior works, QSMA was applied to the global model (i.e. Eq. (1)) for several benchmark structures, including the Brake-Reuβ beam [3], a multi-riveted beam [14], the S4 beam [19, 6], and a 2D representation of the S4 beam [6]. In each of those cases, QSMA estimated the amplitude dependent natural frequency and damping for the mode in question. Optimization was then used to update the parameters of an Iwan joint until the natural frequency and damping of the model matched the measurements. When QSMA is applied to a local model, the modal properties cannot be estimated so a different approach is needed.

3 Methodology

3.1 1 Bolt Truth Model (TM1)

The method is investigated using two different full models, which will be distinguished as truth models. QSMA is performed on each of these truth models to obtain their amplitude dependent frequency and damping, which are used to validate the accuracy of the method. The first truth model is the 2D model described and validated in [6], which will be labeled as *TM1*. It consists of two cantilever beams bolted together at their free ends and can be seen in Figure 5. The geometry of the bolt is simplified, due to the nature of a 2-dimensional model. The nut and bolt were removed and instead the bolt preload is approximated by applying a distributed force over the area that the bolt would occupy. The hole for the bolt was also filled, as the bolt shaft would generally occupy the majority of that space and to preserve the continuity of the model. All other geometry, material properties and mesh refinement can be found in [6], unless otherwise specified here. The preload force used in this work was $446\,\mathrm{N/mm}$ $(2549\,\mathrm{lbf/in})$, which was applied across a 6.35 mm (0.25 in) long surface.

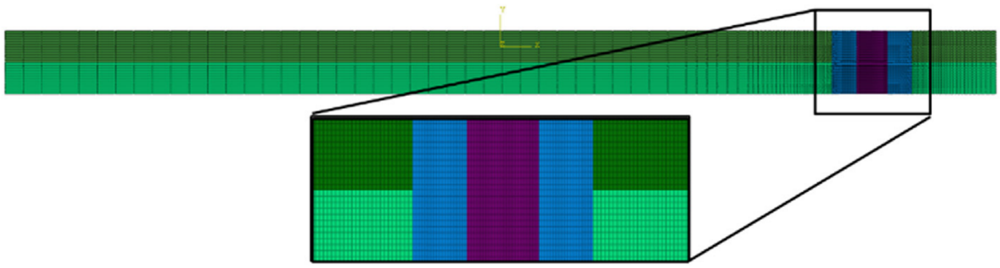

Fig. 5: Two-dimensional bolted beam model used as the first **truth model**, TM1, (described in [6], adapted from [16]), consisting of two cantilever beams, fixed on the left and bolted together at their free ends on the right. The purple region represents the bolt area, and the blue region represents the refined mesh surrounding the bolt.

The first two mode shapes are shown in Figure 6, and are of particular interest, as they contribute shear at the bolt location and are therefore most relevant for evaluating tangential joint behavior. These modes, denoted Mode 1 and 2, are the primary focus for comparison in this work.

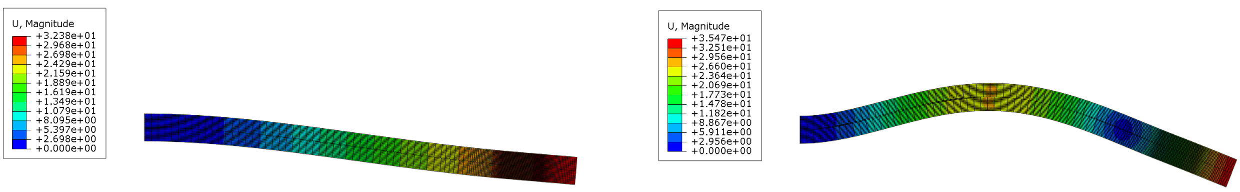

(a) Mode 1 **(b)** Mode 2

Fig. 6: First two mode shapes of the 1 bolt truth model, TM1, as depicted in Figure 5. The colored contour describes the magnitude of the displacement.

3.2 3 Bolt Truth Model (TM3)

The second truth model was developed using the same parameters for the bolted region in TM1. Like the first model, it consists of two cantilever beams, but in this case the beams are three times longer and contain three bolts along their length. This configuration, shown in Figure 7, will be referred to as *TM3*. In essence, the TM3 model is an extension of the TM1 model, with the geometry repeated three times. The bolts are labeled from left to right as A, B and C, with bolt A closest to the fixed end and bolt C at the free end.

Fig. 7: Two-dimensional bolted beam model used as the second **truth model**, TM3. The system consists of two cantilever beams connected by three bolts. The bolts are labeled from left to right as A, B and C.

This second model will demonstrate how the method can be applied to a model with multiple identical joints. A single local model will be used to identify the model for the joint and then it will be applied to all three locations to evaluate the transferability of the joint model. The first two modes of this model can be seen in Figure 8. An additional benefit of the TM3 model is that the mode shapes deform the bolted regions in a more complex shape compared to TM1. For instance, for Mode 1 of TM1, see Figure 6a, the joint generally only experiences bending on the side closer to the fixed end, whereas the two bolts in the center of the TM3 in Mode 2 would experience bending on both sides of the joint. This will be elaborated on later.

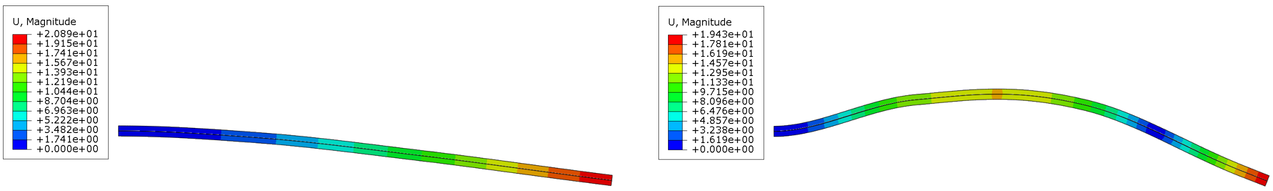

(a) Mode 1

(b) Mode 2

Fig. 8: First two mode shapes of the 3 bolt truth model, TM3, as depicted in Figure 7. The colored contour describes the magnitude of the displacement.

3.3 Local Model

Local joint models were generated in Abaqus by extracting the portion of the truth model surrounding the bolted interface. As the bolt parameters for both TM1 and TM3 are identical, only one local model was created. The cut boundaries were placed $12.7\,\mathrm{mm}$ $(0.5\,\mathrm{in})$ on either side of the bolt center—chosen because it fully captures the contact region and its size matches the optimal uniform RBE3 MPC spider radius identified in [16]. The RBE3 is a type of MPC spider which distributes loads without adding stiffness and [16] showed that the RBE3 spiders performed best when a uniform loading distribution was used. Friction between the upper and lower cut members was modeled using the Lagrange method, with a coefficient of friction of 0.6, matching [6]. A uniform mesh with 5,306 nodes and 5,052 elements was used, slightly finer than the verified truth model [13] in the bolt region. Two uniform RBE3 MPC spider joints were used to connect each side of the contact interface to two separate reference points, located at the contact interface, where the middle of the bolt would be. The bottom reference point was fixed to fully constrain the model. As noted earlier, this allows the displacement to be calculated as the difference between these two reference points as

$$u_r = u_t - u_b \tag{18}$$

where u_t and u_b are the nodal displacements of the top and bottom master nodes respectively and u_r is the relative displacement between both nodes. This configuration can be seen in Figure 3. A clamping or preload force was also applied, with a diameter of $6.35\,\mathrm{mm}$ $(0.25\,\mathrm{in})$, matching that in the truth models previously mentioned.

The local model was quasi-statically loaded by applying a force, F_{eq}, to the top interface node in the direction parallel to the contact interface, as in Figure 3a. This force was linearly ramped ranging from 0 to approximately $1700\,\mathrm{N}$ $(382.2\,\mathrm{lbf})$. Since the bottom master node u_b was grounded, the force in that node was extracted from Abaqus as a reaction force. Note, the upper bound of $1700\,\mathrm{N}$ $(382.2\,\mathrm{lbf})$ corresponds to the onset of macro-slip, which was estimated using the Coulomb friction relationship

$$F_{eq,\max} = \mu F_N \tag{19}$$

where $F_{eq,\max}$, is the maximum shear force at the interface before macro slip, μ is the coefficient of static friction and $F_N = 2832\,\mathrm{N}$ $(636.7\,\mathrm{lbf})$ is the normal preload force. The procedure was then repeated two additional times with the F_{eq} oriented perpendicular to the contact face and with M_{eq}, for the cases in Figures 3b and 3c respectively.

A four-parameter Iwan element was then parameterized to match the force F_{eq} and displacement u_r data of the first set of force-displacement data. The Iwan element [9] was used for this set of data because it is known to accurately capture the nonlinear effects of the sticking and slipping on the contact interface during microslip [20]. The Iwan identification process involved using a particle-swarm, gradient-free optimizer in MATLAB. Specifically the `particleswarm` function [21, 22] that is part of the standard 'Global Optimization Toolbox.' The optimization was defined as

$$\min_{F_s,k_t,\chi,\beta} \sum_{i=1}^{N} \left(u_{iwan,i}(\mathbf{F}_{eq,i}, F_s, k_t, \chi, \beta) - u_{r,i} \right)^2 \tag{20}$$

where the objective function of the optimizer computed the quasi-static response of a single Iwan element, which was grounded at one end and had an applied force applied at its other end. This was evaluated for the i^{th} force measurement that was used in the local model, F_{eq}, where N denotes the number of force samples. Then the sum of square errors were computed, where $\mathbf{u}_{\mathrm{Iwan,i}}$ denotes the i^{th} displacement of the single Iwan element model and $\mathbf{u}_{r,i}$ denotes the i^{th} displacement measured on the local model. The design variables for the optimizer were the parameters of the Iwan element. Specifically the K_t, χ and β. The parameter F_S was set to the onset of macro-slip $F_{eq,\max}$, computed using Eq. (19).

Linear springs in the normal and rotational directions were also identified using the loadings in Figure 3b and 3c. These springs were tuned using the finite-difference of the displacements around equilibrium as

$$k_i = \frac{f_2 - f_1}{x_2 - x_1} \tag{21}$$

where f_1 and f_2 represent forces and x_1 and x_2 represent the displacements of two data points on the force-displacement curve.

The identified Iwan and linear spring parameters are then inserted into the ROM, and QSMA is run to obtain amplitude-dependent frequency and damping for Modes 1 and 2, which are compared against the truth model (see, for example, Figure 10). To quantify how well the ROM captures the truth model, average errors are computed for both frequency and damping. Since damping is inherently difficult to predict, and even experimental measurements can carry uncertainties of 10–20%, a multiplicative error metric is used rather than a standard absolute or relative error. Specifically, the damping error is defined as the ratio of the ROM's predicted damping to the truth damping, averaged across amplitude levels. A ratio of 1 indicates a perfect match; values between 0.1 and 1 indicate underprediction by up to an order of magnitude, while values between 1 and 10 indicate overprediction by up to an order of magnitude. This logarithmic framing is more physically meaningful for damping than a simple percentage error, since damping values are generally estimated with a large margin of uncertainty.

4 Results

4.1 Pure Shear Local Model with Truth Model 1 (TM1)

The first model tested is the *Pure Shear Local Model*, which, as explained in Sec. 2.3, applies an equivalent force F_{eq} to the interface node u_t in the local model in the direction of the spring being tuned. The loading in Figure 3a was used to tune the Iwan element, and the resulting force-displacement curve is compared to the Iwan model in Figure 9a. As can be seen, the model matches the measured data quite well. The loadings in Figures 3b and 3c were used to tune the linear spring perpendicular to the contact interface, as well as the rotational spring. These were obtained by taking the localized slope of the data. This can be seen in Figures 9b and 9c respectively. In practice, only two

Table 1: Tuned linear spring stiffness parameters for ROM. The first set of springs were tuned using the *Pure Shear Local Model*. The second set of springs were tuned with model updating techniques in [16].

	Local Model Tuned		Model Updated	
Parameter	**SI**	**Imperial**	**SI**	**Imperial**
Normal stiffness	3.83×10^6 N/mm	21.9×10^6 lbf/in	45.5×10^9 N/mm	260×10^9 lbf/in
Rotational stiffness	97.6×10^6 N mm/rad	0.864×10^6 lbf in/rad	100×10^6 N mm/rad	0.886×10^6 lbf in/rad

data points are required, but these figures show the behavior over a larger range to establish the range of validity. The normal and rotational linear springs were then identified and can be seen in Table 1.

Linear and Iwan springs were also identified in [16] using the same model as TM1. In contrast, their approach tuned their linear springs by using a model updating strategy that matched the linear natural frequencies. The Iwan was also identified using a model updating strategy, but matched the nonlinear frequency and damping. The linear spring stiffness's are also included in Table 1 for comparison and their Iwan parameters can be found in the Appendix A. Interestingly, the rotational spring in that study is relatively close in value to the spring found in this study. Only a difference of 0.022×10^6 lbf in/rad. However, the spring in the normal direction is different by many orders of magnitude. The Iwan parameters also varied significantly and its response is compared in more detail later in Section 5.3.

These springs were then inserted into the TM1 ROM and the linear modes of the ROM were computed. These were compared with the first six natural frequencies of the truth model, giving an average error of 1.6%. These natural frequencies can be seen in Table B.1 in Appendix B. This shows that this tuning procedure works quite well for creating a ROM that captures the true linear natural frequencies.

QSMA was then performed to predict the amplitude-dependent frequency and damping of the first two modes. As shown in Figure 10, the ROM captured the effective natural frequency quite well for both cases, with an average error of only 0.8% for Mode 1 and 0.5% for Mode 2. The damping prediction was less accurate, under predicting the damping for Modes 1 and 2 by an average multiplicative factor of 0.27 and 0.79 respectively. These results show that while the pure shear approximation provides a reasonable first step, it does not fully capture the nonlinear behavior needed to reproduce the observed damping trends. It also shows that setting the F_s parameter of the Iwan element to the true onset of macro-slip matches the truth data quite well. This can be seen in Figure 10 as the amplitude at which the natural frequency rapidly drops and the damping spikes.

Further comparison between the local model and the truth model revealed notable differences in the contact behavior. The *Pure Shear Local Model* produced a symmetrical stick–slip response on both sides of the joint interface, while the truth model exhibited slippage on only one side, see Figure 11. This asymmetry in the truth model suggests that nonlinear joint behavior is influenced by additional loading mechanisms, particularly bending forces that are absent in the *Pure Shear Local Model*.

Stress distributions from the full FE truth model were examined to support these observations and to guide refinements in defining loading on the local model for subsequent modeling approaches. Similarly, the local model created a symmetrical stress profile, while the stress distribution of the full model was not symmetrical. This motivated the development of more representative local models that incorporate additional loading components beyond the pure shear force used in this model, in order to better capture the asymmetrical stick–slip behavior and the resulting nonlinear modal response.

4.2 Shear-Moment Local Model with Truth Model 1 (TM1)

To account for potential bending moments in the structure, the *Shear-Moment Local Model* was also tested. This model used an equivalent moment, M_{eq}, in addition to the equivalent force, F_{eq}, as described in Sec. 2.3. Both of these loads are applied to the node u_t. The linear stiffness's were tuned well by the previous local model, so only the tuning of the Iwan element is tested by this local model.

For this model, it was assumed that both loads increase proportionately to one another, with α being the ratio between them. Various α ratios were tested, and in each case, a quasi-static analysis was performed and the force-displacement curves were obtained. Then the best Iwan parameters were identified for each. In contrast to the *Pure Shear Local Model*, the Iwan element wasn't able to reproduce the force-displacement curve as well. One example of this can be seen in Figure 12 which compares the force displacement behavior of the tuned Iwan model to that of the local model for the $\alpha = 2.62$ case. As can be seen, the Iwan model did not match at the curve at lower

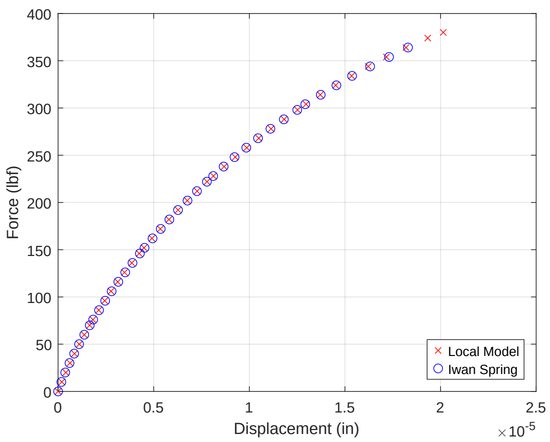

(a) Force displacement data parallel to the contact face, see Figure 3a, along with identified Iwan spring.

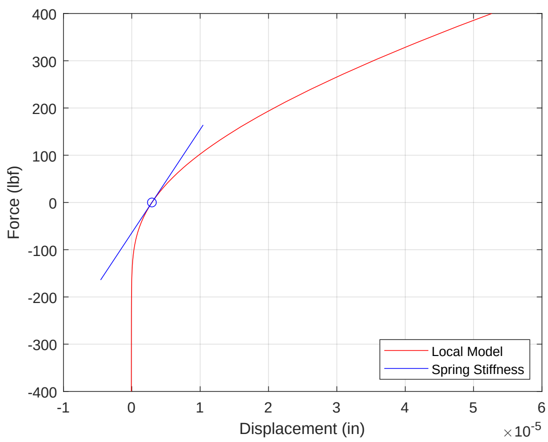

(b) Force displacement data normal to the contact face, see Figure 3b, along with the slope used for the linear spring.

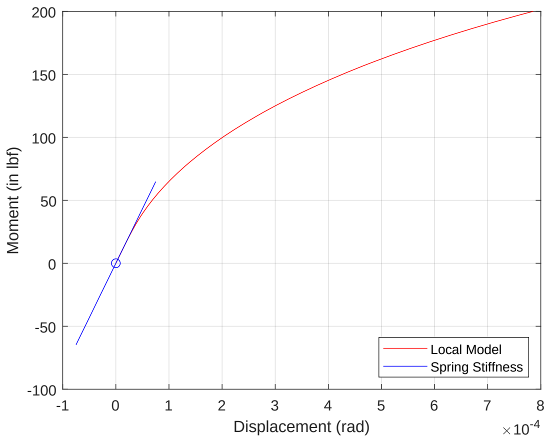

(c) Force displacement data in the rotational direction, see Figure 3c, along with the slope used for the linear spring.

Fig. 9: Force-displacement data extracted from the local model using only an equivalent force, F_{eq} in the corresponding direction.

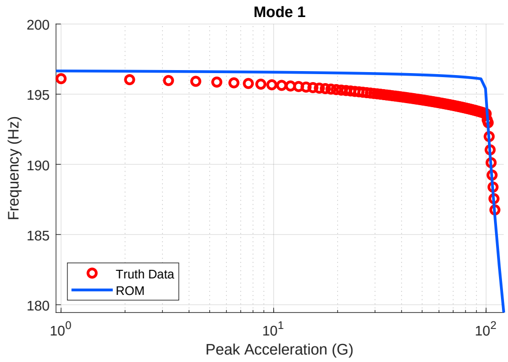

(a) Amplitude dependent frequency of Mode 1

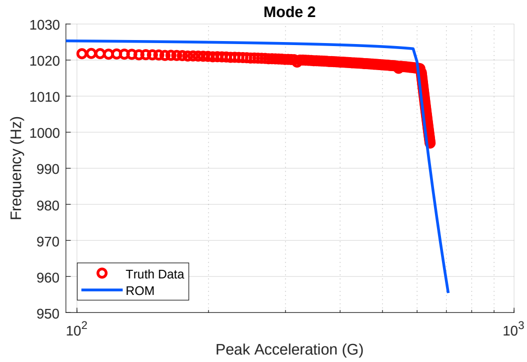

(b) Amplitude dependent frequency of Mode 2

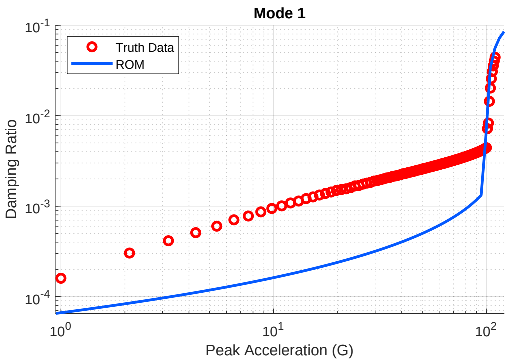

(c) Amplitude dependent damping of Mode 1

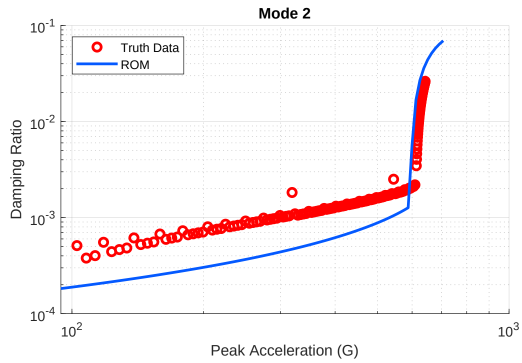

(d) Amplitude dependent damping of Mode 2

Fig. 10: Comparison of nonlinear modal response from the ROM tuned by the *Pure Shear Local Model* (blue) and the TM1 truth model's QSMA results (red circles). The nonlinear response consists of the amplitude dependent frequency and damping of the first two modes. The onset of macro-slip for each mode happens around 100 and 600 G's, respectively, where the natural frequency rapidly drops and the damping spikes.

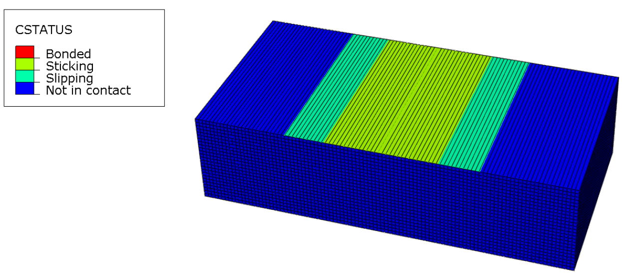

(a) Contour plot showing regions of sticking and slipping in the local model at the load step in which the total contact shear force is $756\,\mathrm{N}$ $(170\,\mathrm{lbf})$. Figure 11b shows how the boundary between stick and slip evolves as load increases. The 2D model was assigned a depth for visualization purposes; the model treats the depth as infinite.

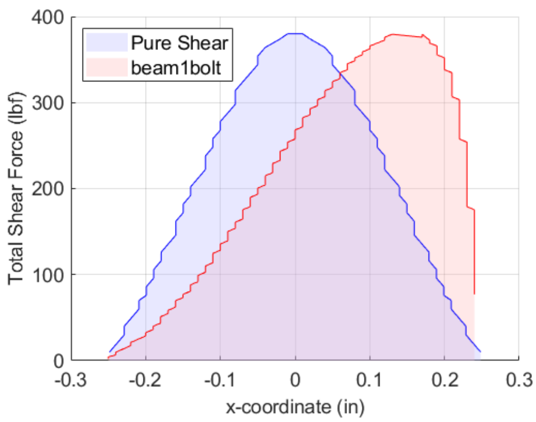

(b) Total shear force at which each point in the contact transitions from sticking to slipping. The behaviors are compared between the local model with the Pure Shear loading and the TM1 truth model (denoted "beam1bolt").

Fig. 11: Comparison of stick and slipping regions in the TM1 model.

displacements nearly as well. This general observation can be made for most of the cases for the *Shear-Moment Local Model*.

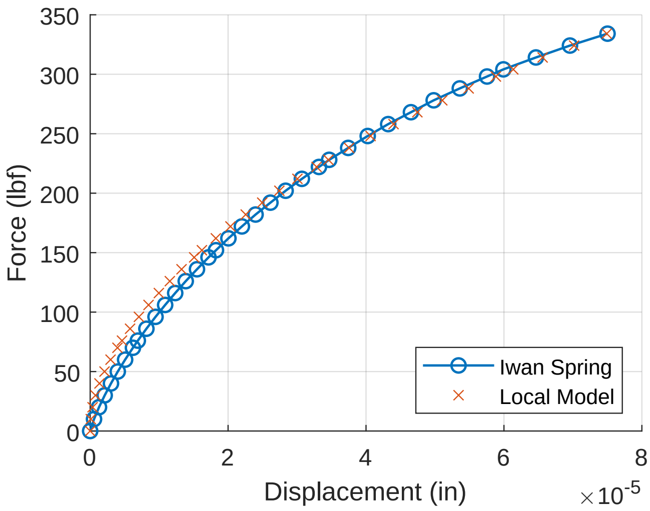

Fig. 12: Force-displacement behavior of the tuned Iwan element compared to the nonlinear force-displacement behavior of the $\alpha = 2.62$ *Shear-Moment Local Model*.

The nonlinear responses for each case are shown in Figure 13 alongside the truth data for the first two modes of TM1. Among those tested, $\alpha = 2.62$ produced the lowest average frequency error for Mode 1 of 0.1% and a damping multiplicative error of 1.12. Interestingly, for Mode 2, not only were the best fit ratios different from Mode 1, they were also different between the frequency and damping fits. The $\alpha = 3.8$ model fit the frequency the best, with 0.3% and 1.52 errors for frequency and damping, while the $\alpha = 5.43$ model fit the damping the best, with errors of 0.5% and 1.16 for frequency and damping respectively. Overall, this method does show that by using both a force and a moment, the local model is able to predict the parameters of the Iwan element more faithfully. Furthermore, while this study reveals the ideal α ratios, there is no way of knowing whether this same ratio would work well on other models. One could seek to approximate it, for example, if the loading $\mathbf{f}_{\text{cut}}$ is uniform over the 0.25 in cross section of the left boundary of the local model and zero elsewhere, then Eq. (13) would give $M_{eq} = (0.125 \text{ in})F_{eq}$, so α =8 in^{-1}. This is, unfortunately, not very close to the ideal values found above. One likely needs to consider the elasticity of the surrounding structure to obtain a reasonable estimate for α.

4.3 Pure Shear Local Model with Truth Model 3 (TM3)

The springs tuned by the *Pure Shear Local Model*, which were identified in 4.1, were then tested on the second truth model, TM3. In this case, the model has three bolted joints, each identical to the joint in TM1 and in the local model. So the Iwan and linear springs that were tuned on the local model can be inserted in place of each of the three bolts in the ROM for TM3.

First, modal analysis is performed on the ROM to test its linear natural frequencies. These frequencies can be found in Table B.2 of Appendix B, and comparing the first six modes with the truth model gives a 1.12% average error. This shows that the linear springs, and the low amplitude K_t of the Iwan element adequately predicted the natural frequencies of the model.

Next, QSMA was performed on the ROM to estimate the nonlinear frequencies and damping of the first two modes. This was run until one of the bolts entered macro slip. These results can be seen in Figure 14 where we can first see that macro-slip is still being capture quite well for both modes. The nonlinear natural frequencies had an average error of about 0.5% for both modes.

This shows that it was able to predict the nonlinear frequencies just as well, if not slightly better, than when it was tested on the TM1 model. The damping was actually predicted significantly better on this truth model, with average errors of 33% and 59% for each mode or a 0.7 or 0.6 average multiplication factor error. All of these statistical values can be found in Appendix C. It is encouraging that this method works so well for predicting the dynamics of this assembly that contains three bolts, each of which is loaded somewhat differently in Modes 1 and 2 than in TM1 or in the local model.

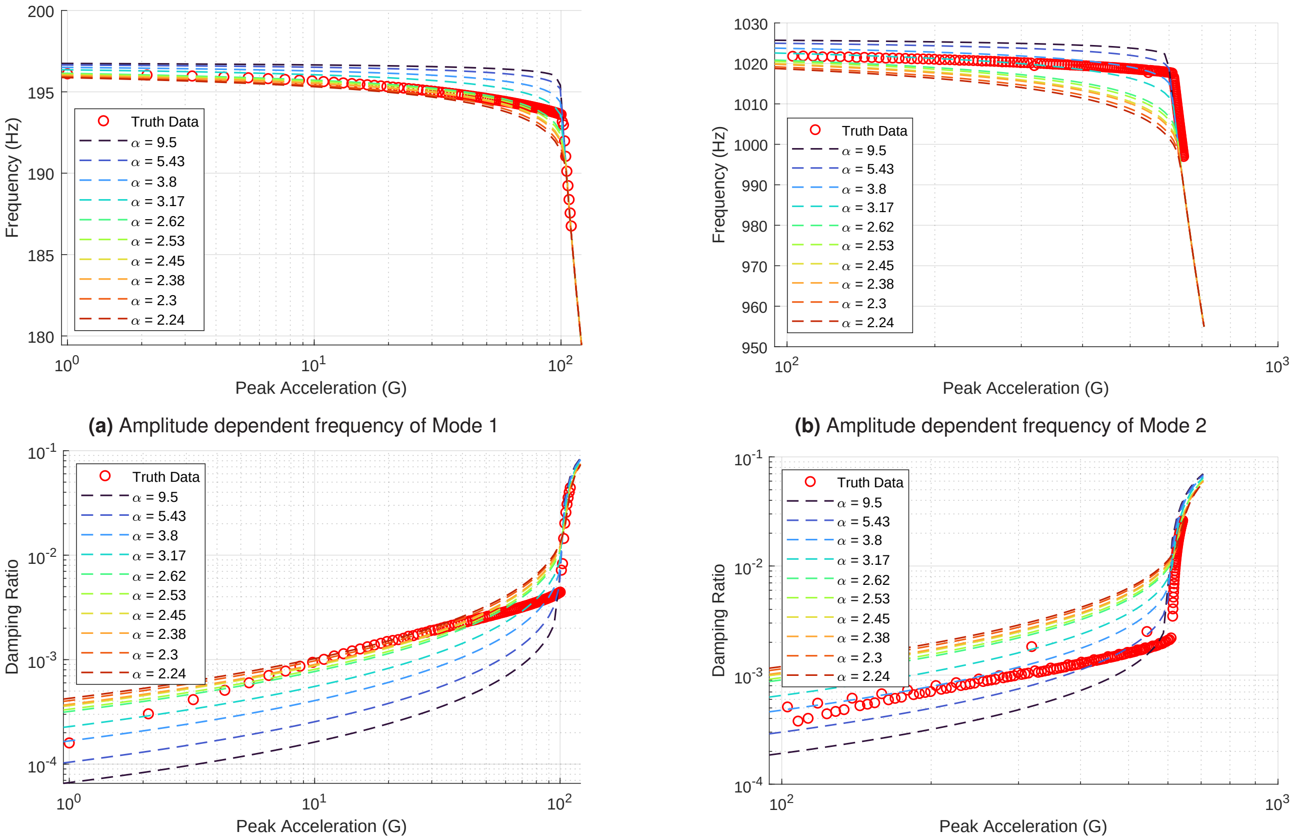

(a) Amplitude dependent frequency of Mode 1

(b) Amplitude dependent frequency of Mode 2

(c) Amplitude dependent damping of Mode 1

(d) Amplitude dependent damping of Mode 2

Fig. 13: Nonlinear modal responses from the ROM's tuned to various *Shear-Moment Local Models* compared against the TM1 truth models' QSMA results for Modes 1 and 2 (red circles). The loading ratios are defined as $\alpha = F/M$, where α has units of in^{-1}. Results arranged in the same format as Fig. 10.

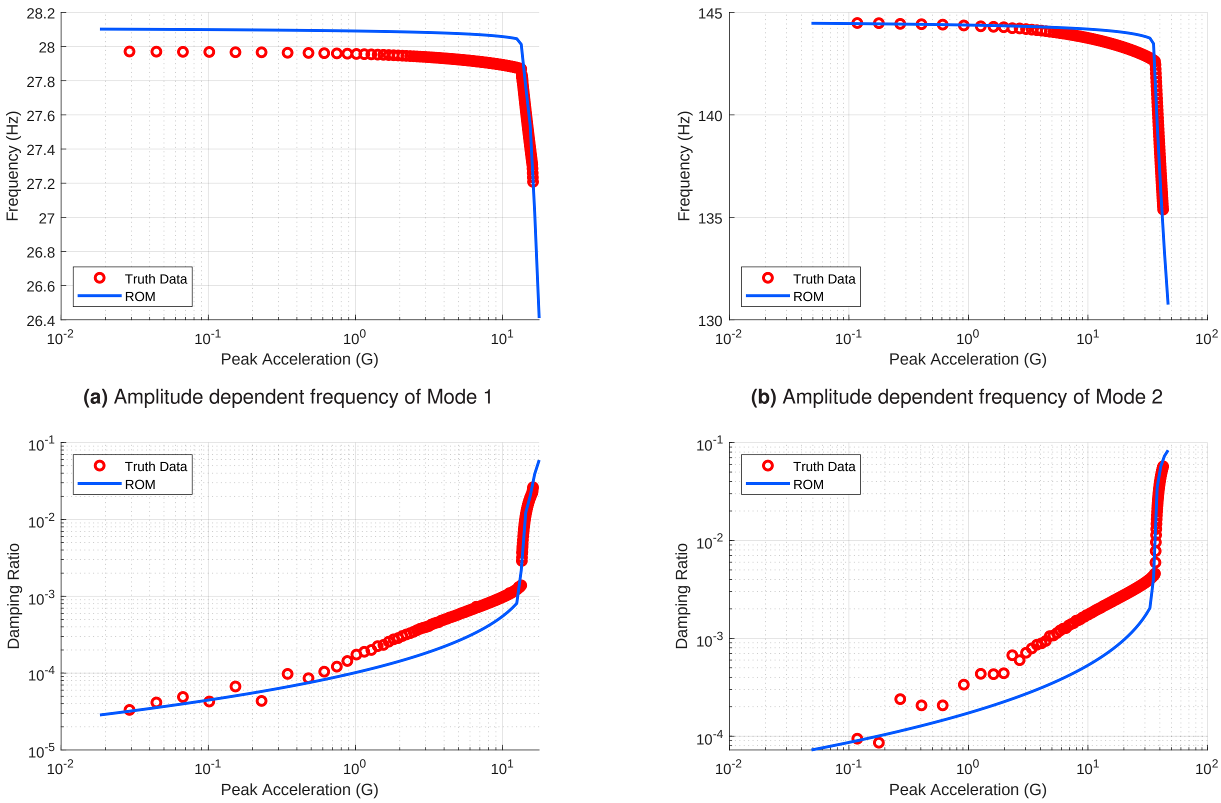

(a) Amplitude dependent frequency of Mode 1

(b) Amplitude dependent frequency of Mode 2

(c) Amplitude dependent damping of Mode 1

(d) Amplitude dependent damping of Mode 2

Fig. 14: Comparison of nonlinear modal response from the ROM of the 3 bolted beam (TM3) tuned by the *Pure Shear Local Model* (blue) against the truth model (red circles), arranged in the same format as Fig. 10. The onset of macro-slip for each mode happens around 10 and 35 G's respectively, where the natural frequency rapidly drops and the damping spikes.

5 Further Observations and Force-Displacement Curve Sensitivity

These results demonstrate that the proposed method consistently under-predicted the damping; however, all predictions remain within an order of magnitude of the truth data. Considering that predicting the damping in bolted interfaces is notoriously difficult, acheiving this level of correlation is significant. Furthermore, from a structural integrity perspective, under predicting damping is preferable to over-predicting it. By underestimating the energy dissipation, the ROM povides a conservative upper bound for vibration amplitudes and stress levels, ensuring that the design remains safe under the predicted worst-case dynamic loading.

Despite the conservative nature of the estimate, the discrepancy prompted further investigation into the sources of the modeling error. To isolate whether these differences arise from the local modeling assumption, where the forces at the cut boundary are approximated as equivalent forces, additional explorations were performed. Force–displacement data was taken directly from the full model, in order to compare the results of the local model with that from an ideal local model. Specifically, QSMA was performed on the global model TM1, with the force ranging up to the onset of macro-slip. Then, the same procedure was applied to the TM3 model, in order to see how these quantities varied between the joints in a model with multiple joints. This provided the true force-displacement curves from the truth models, to compare with those obtained with the local model. A few of these curves were then selected and used to tune the Iwan element, as was done with the local models in the previous section. Since the force displacement data is being extracted from the full model, this would represent data from a perfect local model. In practice this procedure would not be a practial way of tuning a ROM, so it is simply used to further understand the method. Also note, this section will mainly be focused on the data parallel to the contact interface, related to the Iwan element, as the linear springs in the other directions have already been shown to faithfully reproduce the linear natural frequencies.

To extract the force–displacement behavior of the joints from the truth models, uniform RBE3 spiders with $12.7\,\mathrm{mm}$ $(0.5\,\mathrm{in})$ radii were added to both the TM1 and TM3 truth models, so that the terms in Eq. (18) could be estimated. In the truth model the bottom master node u_b is not fixed, as was done in the local models. Additionally, the force in the joint is measured by integrating the total force on the contact surface in the FE model. Since the joint isn't being cut out of the model, the forces at the cut boundary, $\mathbf{F}_{cut}$, do not need to be approximated with an equivalent force, $\mathbf{F}_{eq}$. This integration was performed in Abaqus by outputting the field variable "CFS," which provides the contact frictional force. Only one surface is required, because the top and bottom interfaces carry equal and opposite forces.

These force–displacement curves are compared against one another in Section 5.1 to evaluate the variation that can occur in the data with different local models or different loading scenarios on the full models. Three of these data sets are selected to tune additional ROMs in Section 5.2. In addition, the Iwan parameters used in [16] will also be compared to those obtained here in Section 5.3. Finally, all local force-displacement measurements will be compared in Section 5.4.

5.1 Local Measurements on Full Truth Models

After performing QSMA on models TM1 and TM3 for the first two modes, the force-displacement measurements were extracted at each joint. The force-displacement curves are shown in Figure 15. As can be seen, the plot shows that although all bolts were modeled identically within and across the two truth models, each produced somewhat different force–displacement curves. This is expected, and shows the degree to which the deformation imposed by the surrounding structure shapes the local behavior. The overall range of the variation in the force-displacement curves remains relatively small. For example, the maximum displacements at the onset of macro-slip only range from $760\,\mathrm{nm}$ $(30\times10^{-6}\,\mathrm{in})$ to $1140\,\mathrm{nm}$ $(45\times10^{-6}\,\mathrm{in})$, a difference of only 50%. This illustrates one of the limitations of using a spider and a single four parameter Iwan element to capture the force-displacement behavior. The Iwan element has a constant force-displacement curve that depends only on the relative displacement between the two interface nodes; it is not affected by the other loads on the joint. These results show that the true force-displacement behavior is affected by the loads in the surrounding structure. However, if the fluctuation remains relatively small, the behavior may be considered negligible. This will be investigated in Section 5.2. Note also, that the largest variation observed was between the force-displacement curve of the bolt in TM1 when that structure is loaded in Mode 1 versus Mode 2; TM3 showed about half as much variation across the three bolts and across Modes 1 and 2.

In addition to looking at the force-displacement measurements, the stick and slip profile and the local contact shear were extracted on each of the contact faces for each bolt interface. The contact shear along the profile was plotted on a contour plot for each iteration as the quasi-static load was increased. In addition, the transition point from stick to slip was also plotted on top of the contour plot. Comparing all of the plots together, two representative cases were observed across all the scenarios, which can be seen in Figure 16. For convenience, the nomenclature used in the figure will be referred to here.

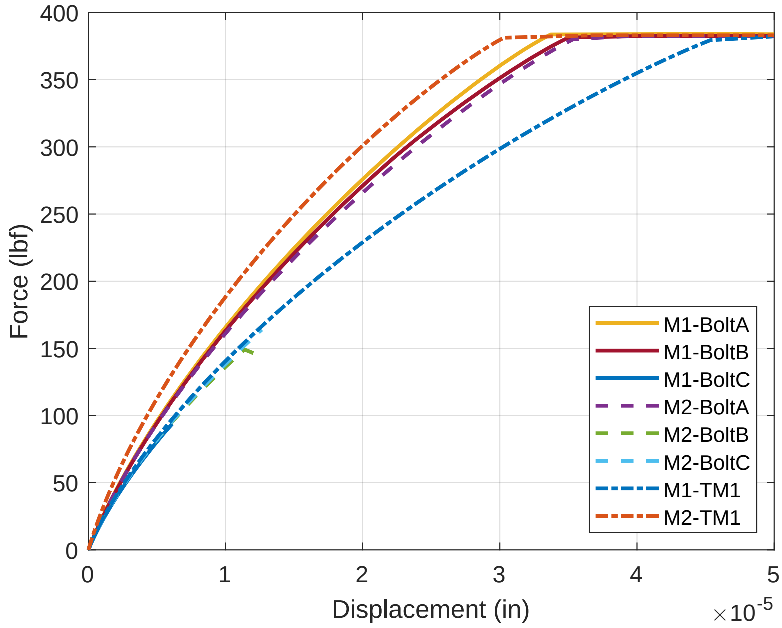

Fig. 15: Force–displacement curves obtained from QSMA applied to the TM1 and TM3 truth models. The legend nomenclature of 'M#–Bolt#' denotes the mode (#) and bolt letter (#) of the TM3 model. For the TM1 model, the bolt is simply referred to as TM1 with the prefix 'M#-' which denotes the mode shape (#).

- **Group 1: One-Sided Slip.** Subfigure 16a illustrates the case of TM1 in Mode 1 (M1-TM), where slippage develops primarily on one side of the contact. Similar behavior was observed in M1-BoltC, M2-BoltB, and M2-BoltC, with only moderate variations between them.
- **Group 2: Two-Sided Slip.** Subfigure 16b shows the case of the first bolt in TM3 in Mode 1 (M1-BoltA), where slippage occurs on both sides of the contact, nearly symmetric about the center. This pattern was also observed in M1-BoltB, M2-BoltA and M2-TM1.

When comparing the groupings in Figure 16 to the corresponding force–displacement curves in Figure 15, a clear correlation can be seen. The bolts exhibiting one-sided slip (Group 1) cluster together in their force–displacement responses, while the two-sided slip (Group 2) cases also form a second, distinct cluster. If the variations in the force–displacement curves shown in Figure 15 are deemed significant, these patterns may provide a means to account for them.

Comparing these to the local models, the *Pure Shear Local Model* experienced the symmetrical behavior of Group 2. This can be seen by comparing its stick-slip transition profile from Figure 11b to 16b. The *Shear-Moment Local Model* acts similarly when its applied moment is significantly small compared to the force. As you lower the force to moment ratio, the transitions to look like Group 1. The force-displacement behaviors of their tuned Iwans are compared in Section 5.4.

5.2 Iwan Elements tuned by Full Models tested on TM1

To test the sensitivity of the nonlinear response to the force-displacement curves, three of the data sets from the truth models were used. The data set M1-TM1 was selected to represent Group 1 where slipping mainly occurred on a single side of the bolt and M1-BoltA was selected to represent Group 2 where slip occurred equally on both sides of the bolt. The third set selected was M2-TM1 since it's force-displacement data varied a bit more in the first group. Each of these curves was then used to identify the Iwan parameters, which can be found in Appendix A. These Iwan elements, as well as the linear springs found earlier, were then inserted into the both ROMs and then QSMA was used to obtain the nonlinear frequency and damping.

In addition to representing the groups of similar force-displacement curves described above, the M1-TM1 and M2-TM1 models are of interest because they capture the exact force-displacement behavior of the truth model in Modes 1 and 2, respectively. Hence, their force displacement curves are the best that could be obtained by a local model, i.e. if the forces, $\mathbf{F}_{cut}$, at the boundaries were known perfectly.

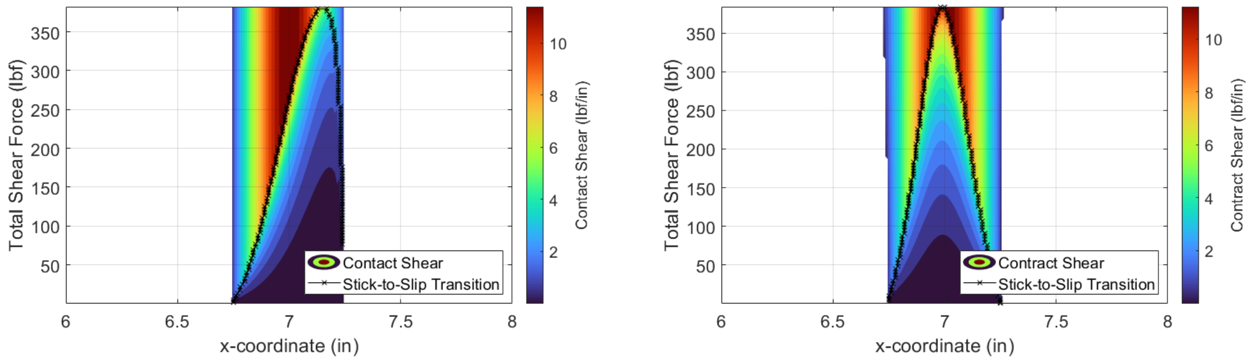

(a) Mode 1 of TM1 (Group 1)
(b) Mode 1, Bolt A of TM3 (Group 2)

Fig. 16: Shear force distributions for two cases. The contour represents shear force at each individual node, while the y-axis shows the total shear force integrated over the contact. Each step in the quasi-static solution provides another row of the contour plot at a progressively higher force. The x-axis represents node location, with the bolt center at $x = 7$ in both sub figures. The overlaid black curve marks the stick–slip boundary: regions below the curve correspond to sticking, and regions above indicate slippage. White areas indicate regions without contact. (a) Group 1: one-sided slip. (b) Group 2: two-sided slip. (Figure 11 provides an alternate visualization for one of these cases.)

These Iwan elements were inserted into the TM1 ROM and then QSMA was performed for the first two modes. The results can be seen in Figure 17. As can be seen, the frequency and damping are closer to the truth data than that which was obtained using the *Pure Shear Local Model* to identify the Iwan parameters. M1-TM1 performed the best by predicting the damping with a multiplication factor of 0.54 and 1.18 for Modes 1 and 2, respectively. Interestingly, M1-TM1 provided better results than M2-TM1 for Mode 2, even though M2-TM1 should technically have the ideal force-displacement relationship for that mode. When it comes to sensitivity, the average frequency error varied from 0.003 to 0.007% while the multiplication factor of damping varied from 0.27 to 1.23. As was the case for the *Pure Shear Local Model*, the damping predictions are within a factor of 4 of the truth data and the macro-slip transition is captured. For comparison, the damping predicted by the *Pure Shear Local Model* had average multiplicative error factors of 0.27 and 0.79 for Modes 1 and 2, respectively. It is surprising that knowing the exact force-displacement relationship for the truth model did not produce a larger improvement in these predictions. It could be that the error in the predictions stems more from the form of the ROM, for example the configuration of the spider constraints and Iwan element, rather than on inaccuracies in the force-displacement behavior.

These Iwan elements were also tested on the TM3 model, and the results can be seen in Figure 18 with all statistics located in Appendix C. As can be seen, M1-TM1 once again gave the best results on average, with an average frequency error of 0.3% and 0.4% for modes 1 and 2 and a damping multiplication factor of 1.18 and 0.97 for Modes 1 and 2, respectively. The one exception to this would be the ROM with the Iwan element identified from the M1-BoltA data from TM3, which gave slightly better frequency error of 0.3% for Mode 2. In addition, as with the test on the TM1 model, all of these Iwan elements predicted the damping within a factor of four and predicted the transition to macro-slip well.

The linear natural frequencies of the ROM were also compared to those from the truth model. For the ROM tuned to M1-TM1, the natural frequencies of the first six modes can be found in Table B.3 in Appendix B and matched with an average error of 0.02%. The ROM tuned to the M2-TM1 data was less accurate, having an average error of 1.02%, as shown in Table B.4 in Appendix B.

5.3 Comparing to Results of the Experimentally Tuned Model (EM)

In [16], study was performed, with a truth model that was nearly identical to TM1 and a ROM similar to that used here. In their study, they used QSMA to predict the frequency and damping of Mode 1 of the truth model, and treated this as experimental data, using optimization to identify the parameters of the Iwan elements. They explored various types of spiders and various spider radii. The Iwan parameters that they obtained for the case that corresponds with this work, specifically the case using RBE3 spiders with a spider radius of 12.3mm (0.5 in), is included in the Appendix A along side all the other Iwan parameters identified in this study.

Figure 17 also shows the result when the Iwan Element from [16] is inserted into the TM1 ROM. As can be seen, the ROM with their Iwan parameters performs exceptionally well for Mode 1 at low vibration amplitudes; it was tuned

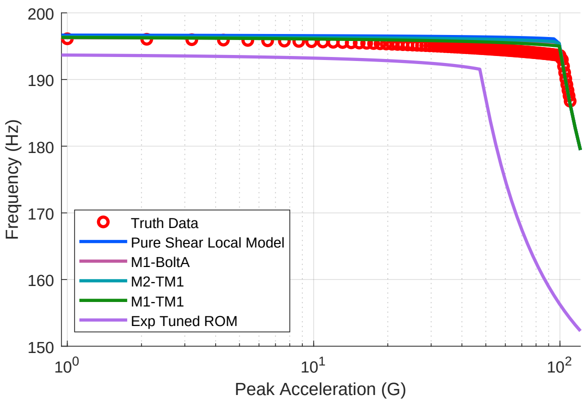

(a) Amplitude dependent frequency of Mode 1

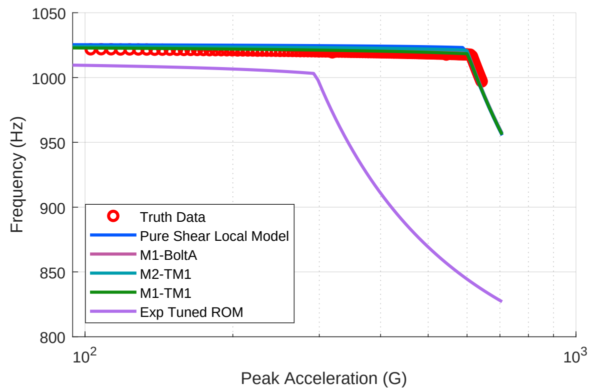

(b) Amplitude dependent frequency of Mode 2

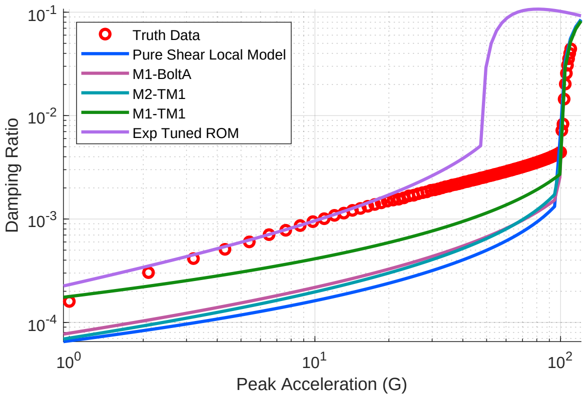

(c) Amplitude dependent damping of Mode 1

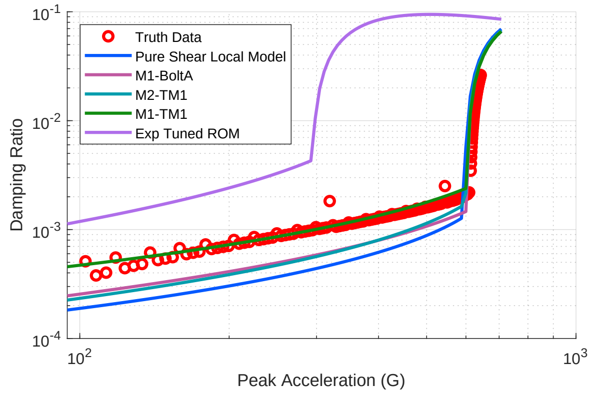

(d) Amplitude dependent damping of Mode 2

Fig. 17: Comparison of modal frequency and damping responses between Mode 1 and 2 of the TM1 truth model, where the Iwan element in the ROM was tuned to three different force-displacement curves. Force-displacement curves M1-TM1, M2-TM1, and M1-BoltA from Figure 15 were used to identify Iwan elements in each of the ROMs, respectively. These data sets represent local measurements taken from the truth models instead of local models. Results for the *Pure Shear Local Modal*, in Figure 10, are also included for comparison.

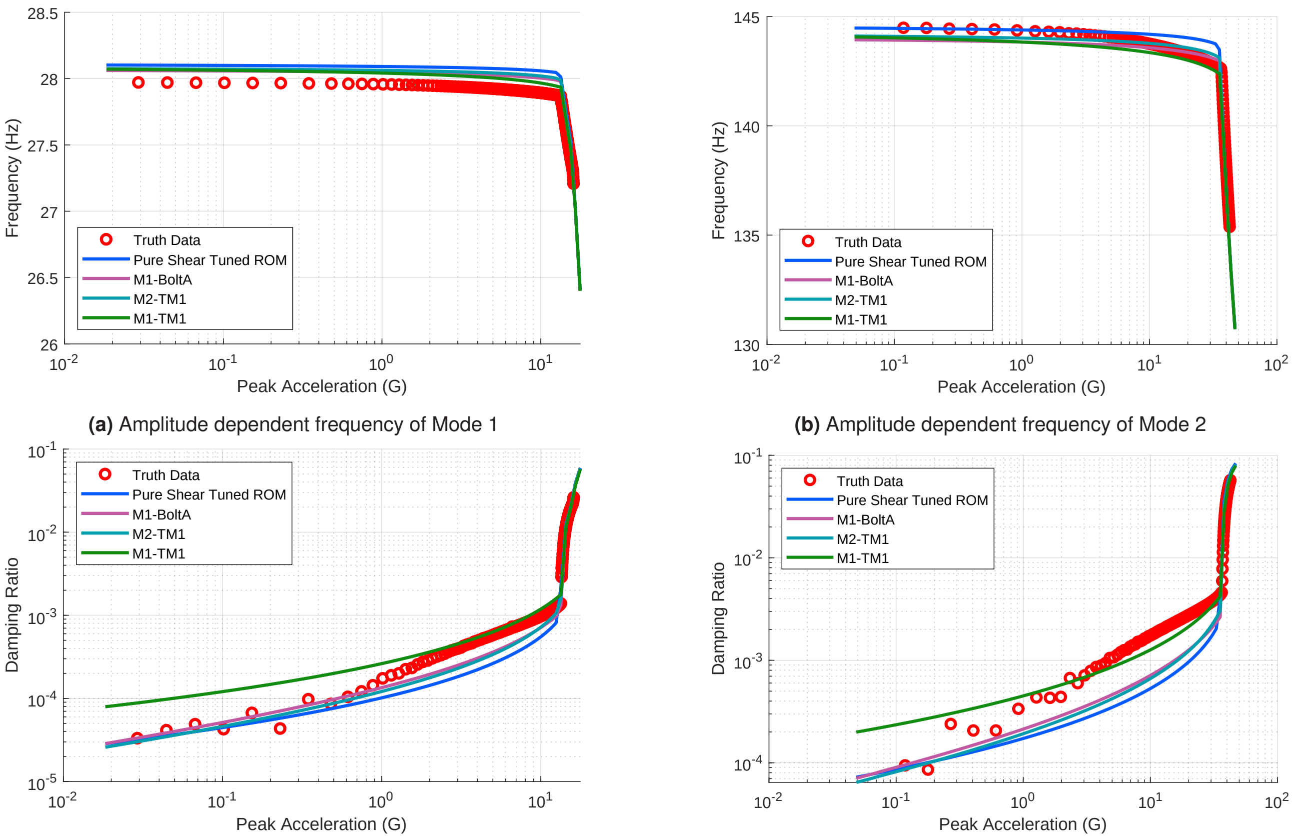

(a) Amplitude dependent frequency of Mode 1

(b) Amplitude dependent frequency of Mode 2

(c) Amplitude dependent damping of Mode 1

(d) Amplitude dependent damping of Mode 2

Fig. 18: Comparison of modal frequency and damping responses between Mode 1 and 2 of the TM1 truth model, where the Iwan element in the ROM was tuned to three different force-displacement curves. Force-displacement curves M1-TM1, M2-TM1, and M1-BoltA from Figure 15 were used to identify Iwan elements in each of the ROMs, respectively. These data sets represent local measurements taken from the truth models instead of local models. Results for the *Pure Shear Local Modal*, in Figure 10, are also included for comparison.

using only simulated measurements of Mode 1 below 20 g peak acceleration. On the other hand, their model does not capture the transition to macro-slip. Their ROM also struggled to predict the behavior of Mode 2, over predicted the damping and greatly under-predicting the force at which macro-slip occurs. The model from [16] over-predicts the damping for Mode 2 by a factor of 2 to 4, whereas the *Pure Shear Local Model* under-predicted the damping by an average factor of 0.79.

In general, lowering the macro-slip force in an Iwan element allows it to dissipate more energy, increasing the damping. The comparison in Figure 17 prompted the question: Could the local models obtain better predictions of the damping if the macro-slip force was allowed to decrease? This was explored, but no case was found in which the damping predictions improved significantly, without inducing significant errors in force-displacement behavior of the Iwan element, which is elaborated in Figure 19.

5.4 Comparing Force-Displacement Curves

For further comparison, the force-displacement measurements from the local models, the three truth models and that from the IWan element from [16] are compared in Figure 15. A few observations can be made:

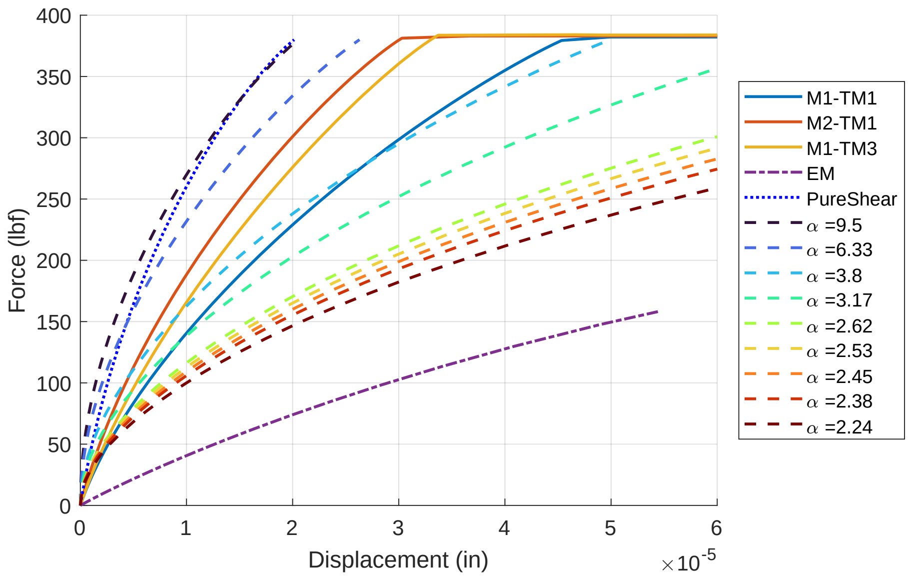

Fig. 19: Force–displacement curves obtained from QSMA applied to the TM1 and TM3 truth models, compared with local joint models and the ROM tuned to experimental data (EM) in [16].

- First, all the curves from the truth models and the local models differ substantially from the force-displacement behavior obtained using the Iwan parameters in EM [16].
- Second, the *Pure Shear Local Model* falls outside the range of the truth model curves. However, its interesting to note that the *Pure Shear Local Model* falls nearest to the Group 2 truth curves, which also produce symmetrical slip profiles, although it still differs by quite a bit.
- Third, the *Shear–Moment Local Models* that gave the best predictions of damping (i.e. $\alpha = 2.62$). However, they do not match either the truth model or the model from [16], although they do lie between the two.

The first observation is especially significant. The ROM in that work was able to match the nonlinear frequency and damping curves of Mode 1 very well, yet it does not accurately capture the local force-displacement behavior of the joint.

6 Conclusion

This work proposed a new strategy for predicting the nonlinear damping due to bolted joints in a structure. In the proposed approach, a reduced-order model (ROM) was built where the bolted joint is represented as a four-parameter

Iwan element. The element was tuned to the behavior of the bolt by a small local model of the joint that is finely meshed with its nonlinear physics, such as friction, is defined. The force-displacement behavior of this model is used to identify an Iwan element to capture the nonlinear behavior of the joint in a ROM. This differs from prior works, which used optimization to tune the ROM to reproduce the amplitude-dependent frequency and damping behavior [3, 13], or used a detailed model of the entire structure to predict the nonlinear behavior due to the joints [6, 7].

Two methods were explored for formulating the local model. They were tested on two different truth models. The first formulation applied only an equivalent force at the location of the bolt. This approach produced a ROM that was able to match the linear natural frequencies of the first six modes with an average error of 1.4% between the two truth models. The nonlinear frequency was predicted with an average error of 0.8% and 0.5% for both truth models. The damping prediction was less accurate, under predicting it during micro-slip. However, it did accurately predict the transition to macro-slip for both the nonlinear frequency and damping. In addition, since lower damping corresponds to a higher amplitudes at resonance, under predicting the damping, as apposed to over-predicting, indicates the method is conservative in its results.

The second formulation incorporated an equivalent moment in addition to the equivalent force. With the additional load, the model was no longer predictive, so it was evaluated at a variety of different force to moment ratios. The best ratio was identified and showed that it matched the nonlinear data better. This showed that the local model can obtain better results with a better estimate for the approximation of the forces at the cut boundary.

Further investigation in the method was also pursued by taking equivalent measurements on the full model as was done on the local models. This showed that the force-displacement behavior did not vary much, meaning the Iwan element could reasonably approximate the behavior. Three of these data sets from the full model were then tested with the methodology, as opposed to using the local model measurements. This showed the sensitivity of the nonlinear results to the force-displacement curve as well as showing the error caused by approximated the forces at the cut boundary. Better predictions were obtained, though the damping was still under-predicted.

The method was also compared to results found from past works that used model updating to tune the Iwan element [16]. This showed that this method was not able to match the damping data used as the reference data for model updating nearly as well, however, this method was more consistent in predicting the transition from micro-slip to macro-slip as well as predicting the damping that was not used as reference data for model updating. This method under-predicted the damping, whereas the model updating approach could over predict the damping. Showing that this method is a more conservative approach.

Interestingly, the method preformed better on the truth model with multiple bolted joints. The proposed approach is most appealing for structures that contain many bolts; it would be completely infeasible to predict the damping of a structure with hundreds of joints using the best available approaches (e.g. [6, 7, 5]), yet the approach in this work could readily address a structure with many joints, producing a computationally efficient ROM.

The current work focused on developing the method using a 2-dimensional model. It is anticipated that similar results would be obtained using a 3-dimensional model, however, further testing would be needed to verify this. It would be interesting to see how those results would compare to the results in this work, both in nonlinear predictions as well as local force-displacement measurements.

References

[1] H. Festjens, G. Chevallier, and J.-L. Dion. A numerical tool for the design of assembled structures under dynamic loads. *International Journal of Mechanical Sciences*, 75:170–177, 2013. ISSN 00207403. doi:10.1016/j.ijmecsci.2013.06.013.

[2] P. Papanikos, S. Meguid, and Z. Stjepanovic. Three-dimensional nonlinear finite element analysis of dovetail joints in aeroengine discs. *Finite Elements in Analysis and Design*, 29:173–186, 1998.

[3] R. M. Lacayo and M. S. Allen. Updating Structural Models Containing Nonlinear Iwan Joints Using Quasi-Static Modal Analysis. *Mechanical Systems and Signal Processing*, 118(1 March 2019):133–157, 2019. doi:https://doi.org/10.1016/j.ymssp.2018.08.034. Number: 1 March 2019.

[4] M. S. Allen, R. Lacayo, and M. R. Brake. Quasi-static Modal Analysis based on Implicit Condensation for Structures with Nonlinear Joints. September 2016.

[5] S. Baek and B. Epureanu. Reduced-Order Modeling of Bladed Disks With Friction Ring Dampers. *Journal of Vibration and Acoustics*, 139(061011), August 2017. ISSN 1048-9002. doi:10.1115/1.4036952.

[6] E. Jewell, M. S. Allen, I. Zare, and M. Wall. Application of Quasi-Static Modal Analysis to a Finite Element Model and Experimental Correlation. *Journal of Sound and Vibration*, 479(4 August):115376, 2020, URL https://doi.org/10.1016/j.jsv.2020.115376. Number: 4 August.

[7] S. I. Zare Estakhraji, M. Wall, J. Capito, and M. S. Allen. A thorough comparison between measurements and predictions of the amplitude dependent natural frequencies and damping of a bolted structure. *Journal of Sound and Vibration*, 544:117397, February 2023. ISSN 0022-460X. doi:10.1016/j.jsv.2022.117397.

[8] J. P. Winkel, V. J. Suarez, and J. C. Akers. Combined Qualification Vibration Testing and Fixed Base Modal Testing Utilizing a Fixed Based Correction Method. Orlando, FL, 2020.

[9] D. J. Segalman. A Four-Parameter Iwan Model for Lap-Type Joints. *Journal of Applied Mechanics*, 72(5):752–760, February 2005. ISSN 0021-8936. doi:10.1115/1.1989354.

[10] W. C. Hurty. Dynamic analysis of structural systems using component modes. *AIAA Journal*, 3(4):678–685, April 1965. ISSN 0001-1452. doi:10.2514/3.2947. Number: 4.

[11] R. J. Craig and M. Bampton. Coupling of Substructures for Dynamic Analysis. *AIAA Journal*, 6(7):1313–1319, 1968. doi:10.2514/3.4741. Number: 7.

[12] M. S. Allen, D. Rixen, M. Van Der Seijs, P. Tiso, T. Abrahamsson, et al. *Substructuring in Engineering Dynamics: Emerging Numerical and Experimental Techniques*. Springer, CISM International Centre for Mechanical Sciences, 2020. ISBN 978-3-030-25531-2, URL https://doi.org/10.1007/978-3-030-25532-9.

[13] A. Singh, Wall, Mitchell, Allen, Matthew S., and Kuether, Robert J. Spider Configurations for Models with Discrete Iwan Elements. In *Nonlinear Structures and Systems*, volume 1, pages 25–38, Orlando, Florida, January 2019. Springer.

[14] Blackham, Joshua, Stoker, Cameron, Allen, Matthew S., and Rapp, Brandon. Nonlinear Model Updating for Riveted Joints. In *Proceedings of the 43rd International Modal Analysis Conference*, Orlando, FL, February 2025.

[15] B. Rapp, D. Griffiths, and R. Hutchinson. Aerospace Applications of Quasi Static Modal Analysis with Riveted Joints. In *44th International Modal Analysis Conference (IMAC XLIV)*, Palm Springs, CA, USA, 2026.

[16] Bahr, Brennan, Crapo, Benjamin, Allen, Matthew S., and Joshua, Raymond. Comparing Multi-Point Constraints in Nonlinear Modeling of a Two-Dimensional Beam. In *43rd International Modal Analysis Conference (IMAC XLIII)*, Orlando, FL, United states, February 2025.

[17] Simulia. Abaqus analysis user's guide, 2024, URL https://www.3ds.com/products/simulia.

[18] D. Shetty and M. S. Allen. Fast Simulation of a Single Degree-of-Freedom system consisting of an Iwan element using the Method of Averaging. *ASME Journal of Vibrations and Acoustics*, 142(5), October 2020. doi:https://doi.org/10.1115/1.4047070.

[19] Singh, Aabhas. *Multi-Mode Quasi-Static Loading and Interface Reduction to Model Joint Nonlinearity*. PhD thesis, University of Wisconsin-Madison, Madison, WI, June 2021.

[20] D. J. Segalman, D. L. Gregory, M. J. Starr, B. R. Resor, M. D. Jew, et al. Handbook on Dynamics of Jointed Structures. Technical Report SAND2009-4164, Sandia National Laboratories, Albuquerque, NM 87185, 2009.

[21] The MathWorks, Inc. *particleswarm - Particle Swarm Optimization*. MathWorks, Natick, Massachusetts, 2025, URL https://www.mathworks.com/help/gads/particleswarm.html. Accessed: 2025-09-25.

[22] J. Kennedy and R. Eberhart. Particle swarm optimization. In *Proceedings of ICNN'95 - International Conference on Neural Networks*, volume 4, pages 1942–1948 vol.4, 1995. doi:10.1109/ICNN.1995.488968.

Appendix

Appendices

This appendix provides the supporting technical data and validation metrics for the reduced-order models (ROMs) discussed in the preceding chapters. Appendix A lists the parameters for all the four-parameter Iwan elements, including those tuned via the Pure Shear and Shear-Moment local models. To quantify the accuracy of these representations, Appendix B details the linear natural frequency errors relative to the truth models, while Appendix C provides a comparison of nonlinear frequency and damping.

A All Tuned Parameters for the Four Parameter Iwan Elements

Table A.1: Tuned Four Parameter Iwan Elements for each dataset mentioned in this study. Models designated with an α value corresponds to the *Shear-Moment Local Model* defined in the paper. The Iwan parameters labeled as 'Experimental Data' was tuned in another work, [16]

	$\mathbf{F_s}$		$\mathbf{K_t}$			
Model	**N**	**lbf**	**N/mm**	**lbf/in**	χ	β
Pure Shear	1700	382	2.08e+07	1.19e+08	-0.8927	7.20e-02
α = 9.5	1700	382	3.87e+08	2.21e+09	-0.9939	1.00e-05
α = 5.43	1700	382	2.35e+08	1.34e+09	-0.9936	1.09e-05
α = 3.8	1700	382	2.03e+08	1.16e+09	-0.9954	1.82e-05
α = 3.17	1700	382	1.70e+08	9.68e+08	-0.9960	1.24e-05
α = 2.62	1700	382	1.61e+08	9.18e+08	-0.9970	1.54e-05
α = 2.53	1700	382	1.35e+08	7.70e+08	-0.9966	1.32e-05
α = 2.45	1700	382	2.35e+08	1.34e+09	-0.9982	1.00e-05
α = 2.38	1700	382	3.41e+08	1.95e+09	-0.9988	1.06e-05
α = 2.3	1700	382	1.71e+08	9.79e+08	-0.9978	1.07e-05
α = 2.24	1700	382	1.23e+08	7.05e+08	-0.9971	1.36e-05
M1-TM1	1700	382	1.09e+07	6.22e+07	-0.9272	7.55e-02
M2-TM2	1700	382	6.60e+06	3.77e+07	-0.7385	1.76e-01
M1-boltA	1700	382	5.16e+06	2.95e+07	-0.7245	2.82e-01
Experimental Data	782	176	8.76e+05	5.00e+06	-0.5260	4.97e-01

B Linear Error Fit Metrics of All Models

Table B.1: First 6 linear natural frequencies of the TM1 ROM tuned by the *Pure Shear Local Model* compared to truth natural frequencies of the TM1 truth model. Matched with a 1.59% average error.

Mode	Truth Freq (Hz)	ROM Freq (Hz)	Error (%)
1	196.2	196.8	0.30
2	1023.1	1026.4	0.32
3	1143.8	1178.9	3.07
4	2503.6	2491.1	0.50
5	3135.7	3243.6	3.44
6	4666.2	4576.8	1.92

Table B.2: First 6 linear natural frequencies of the TM3 ROM tuned by the *Pure Shear Model* compared to truth natural frequencies of the TM3 truth model. Matched with a 1.12% average error.

Mode	Truth Freq (Hz)	ROM Freq (Hz)	Error (%)
1	28.0	28.1	0.26
2	144.3	144.6	0.18
3	314.8	307.6	2.30
4	735.7	740.0	0.59
5	885.2	876.0	1.04
6	886.1	907.1	2.37

Table B.3: First 6 linear natural frequencies of the TM1 ROM tuned by the *M1-TM1* compared to truth natural frequencies of the TM1 truth model. Matched with a 0.02% average error.

Mode	Truth Freq (Hz)	ROM Freq (Hz)	Error (%)
1	196.2	196.6	0.002
2	1023.1	1025.8	0.003
3	1143.8	1178.9	0.031
4	2503.6	2490.6	0.005
5	3135.7	3243.6	0.034
6	4666.2	4576.6	0.019

Table B.4: First 6 linear natural frequencies of the TM3 ROM tuned by the *M1-TM1* compared to truth natural frequencies of the TM3 truth model. Matched with a 1.06% average error.

Mode	Truth Freq (Hz)	ROM Freq (Hz)	Error (%)
1	28.0	28.1	0.21
2	144.3	144.4	0.06
3	314.8	307.4	2.34
4	735.7	738.3	0.35
5	885.2	876.0	1.04
6	886.1	907.1	2.37

C Error Fit Metrics of All Models

Table C.1: Error metrics for all tuned ROMs considered in this study matching Mode 1. Models designated with an α value corresponds ROMs that were tuned by the corresponding *Shear-Moment Local Model* defined in the paper. The frequency and damping errors are computed by taking the mean of the difference between the true value and the ROM, divided by that of the ROM. The multiplication factor is computed by taking the geometric mean of the ratios of the ROM over the truth model.

ROM Model	Tuned by Model	Frequency Error (%)	Damping Error (%)	Damping Mult. Factor
Bolted Beam (TM1)	Pure Shear	0.802	76.00	0.27
Bolted Beam (TM1)	α = 9.5	0.826	72.91	0.30
Bolted Beam (TM1)	α = 5.43	0.703	59.85	0.44
Bolted Beam (TM1)	α = 3.8	0.498	42.96	0.66
Bolted Beam (TM1)	α = 3.17	0.306	33.59	0.85
Bolted Beam (TM1)	α = 2.62	0.129	31.88	1.12
Bolted Beam (TM1)	α = 2.53	0.129	32.94	1.16
Bolted Beam (TM1)	α = 2.45	0.179	35.98	1.24
Bolted Beam (TM1)	α = 2.38	0.212	37.55	1.26
Bolted Beam (TM1)	α = 2.3	0.315	43.34	1.35
Bolted Beam (TM1)	α = 2.24	0.386	48.62	1.40
Bolted Beam (TM1)	M1-TM1	0.466	50.93	0.54
Bolted Beam (TM1)	M2-TM1	0.653	69.99	0.33
Bolted Beam (TM1)	M1-BoltA	0.590	69.58	0.33
Bolted Beam (TM1)	Model Updated	8.778	1316.26	6.21
3 Bolt Beam (TM3)	Pure Shear	0.509	32.95	0.71
3 Bolt Beam (TM3)	M1-TM1	0.264	22.23	1.18
3 Bolt Beam (TM3)	M2-TM1	0.400	22.01	0.80
3 Bolt Beam (TM3)	M1-BoltA	0.355	21.15	0.81

Table C.2: Error metrics for all tuned ROMs considered in this study matching Mode 2. Models designated with an α value corresponds ROMs that were tuned by the corresponding *Shear-Moment Local Model* defined in the paper. The frequency and damping errors are computed by taking the mean of the difference between the true value and the ROM. The multiplication factor is computed by taking the geometric mean of the ratios of the ROM against the truth values.

ROM Model	Tuned by Model	Frequency Error (%)	Damping Error (%)	Damping Mult. Factor
Bolted Beam (TM1)	Pure Shear	0.518	78.16	0.79
Bolted Beam (TM1)	α = 9.5	0.547	75.29	0.89
Bolted Beam (TM1)	α = 5.43	0.455	56.81	1.16
Bolted Beam (TM1)	α = 3.8	0.327	61.69	1.52
Bolted Beam (TM1)	α = 3.17	0.332	86.36	1.79
Bolted Beam (TM1)	α = 2.62	0.559	127.15	2.11
Bolted Beam (TM1)	α = 2.53	0.602	134.17	2.15
Bolted Beam (TM1)	α = 2.45	0.679	146.92	2.24
Bolted Beam (TM1)	α = 2.38	0.711	152.05	2.28
Bolted Beam (TM1)	α = 2.3	0.809	167.53	2.38
Bolted Beam (TM1)	α = 2.24	0.874	178.12	2.45
Bolted Beam (TM1)	M1-TM1	0.262	31.75	1.23
Bolted Beam (TM1)	M2-TM1	0.378	56.70	0.88
Bolted Beam (TM1)	M1-BoltA	0.321	53.24	0.86
Bolted Beam (TM1)	Model Updated	10.739	2596.30	13.79
3 Bolt Beam (TM3)	Pure Shear	0.502	59.13	0.59
3 Bolt Beam (TM3)	M1-TM1	0.413	26.63	0.97
3 Bolt Beam (TM3)	M2-TM1	0.344	49.56	0.66
3 Bolt Beam (TM3)	M1-BoltA	0.322	47.55	0.67